Multiscale mechanistic modelling of the host defense in invasive aspergillosis reveals leukocyte activation and iron acquisition as drivers of infection outcome

Henrique AL Ribeiro[1], Luis Sordo Vieira[1,2], Yogesh Scindia[1, 5], Bandita Adhikari[3], Matthew Wheeler [1], Adam Knapp[1], William Schroeder[4], Borna Mehrad[1, ‡], Reinhard Laubenbacher[1*, ‡]

1 Division of Pulmonary, Critical Care, and Sleep Medicine, Department of Medicine, University of Florida, Gainesville, FL, USA
2 Department of Psychiatry, University of Florida, Gainesville, FL, USA
3 Center for Quantitative Medicine, School of Medicine, University of Connecticut, Farmington, CT, USA
4 Kitware Inc., Clifton Park, NY, USA
5 Department of Pathology, University of Florida, Gainesville, FL, USA

* reinhard.laubenbacher@medicine.ufl.edu
‡Co-last authors

Keywords: *Aspergillus fumigatus*, innate immune response, iron homeostasis, computational model

Abstract

Aspergillus species are ubiquitous environmental molds, the spores of which are inhaled daily by most humans. Immunocompromised hosts can develop an invasive infection resulting in high mortality. There is, therefore, a pressing need for host-centric therapeutics for this infection. To address this need, we created a multi-scale computational model of the infection, focused on its interaction with the innate immune system and iron, a critical nutrient for the pathogen. The model, parameterized using published data, was found to recapitulate a wide range of biological features and was experimentally validated *in vivo*. Conidial swelling was identified as critical in fungal strains with high growth, whereas the siderophore secretion rate is an essential prerequisite for establishment of the infection in low-growth strains. In immunocompetent hosts, high growth, high swelling probability, and impaired leukocyte activation lead to a high conidial germination rate. Similarly, in neutropenic mice, high fungal growth was achieved through synergy between high growth rate, high swelling probability, slow leukocyte activation, and high siderophore secretion. In summary, the model reveals a small set of parameters related to fungal growth, iron acquisition, and leukocyte activation as key determinants of the fate of the infection.

Introduction

Invasive aspergillosis is a human infection with increasing incidence, related to the use of immunosuppressive therapies, such as cancer chemotherapy and immunosuppression medications [1]. More recently, it has also been observed that 10% to 14% of critically ill patients with COVID-19 developed invasive aspergillosis [2, 3]. Mortality remains high, 30-60% in recent surveys [4], despite advances in diagnostics and therapy. Increasing triazole resistance in this infection [5] has raised the specter of a "perfect storm" [6] in an increasing population of susceptible individuals with a diminished repertoire of treatment options.

The research presented here was motivated by the search for host-centric interventions in immuno-compromised patients that can be used in combination with antifungal treatments. An important mechanism in innate immunity is the sequestration of iron from pathogens, a nutrient critical for nearly all organisms. A well-established literature supports the concept that the "battle over iron" is characteristic of the host's attempt to attenuate microbial growth during many infections [7]. Iron is particularly relevant to the pathogenesis of aspergillosis [8]. The iron sequestration feature of the innate immune response involves several intertwined processes that unfold across spatial and temporal scales. This makes it challenging to assess the effect of perturbations of individual mechanisms on infection dynamics. A computational model that captures the key mechanisms, broadly reflects the underlying immune biology, and is well-validated, can play an essential role in hypothesis generation and the discovery of emergent properties of the immune response.

Several models related to respiratory *Aspergillus* infections and their pathology have been previously published. For example, agent-based models have shown the necessity of chemotactic signals for proper fungal clearance [9, 10]. Our own work includes a model of the innate immune response to *A. fumigatus*, showing that a key determinant of infection is the range at which macrophages can detect the fungus [11], and an intracellular regulatory network linking iron metabolism to oxidative stress in a fungal cell [12]. The model presented here is parameterized entirely with information from the literature, rather than through data fitting, and is validated by showing that it can recapitulate a wide range of experimental data and features reported in the literature that were not used in its construction, as well as experimental data generated for the purpose of model validation. The model was then used to identify major drivers of the growth of fungal burden, providing potential targets for intervention.

Materials and methods

A computational model of the immune response to invasive aspergillosis

The model is an agent-based model of invasive pulmonary aspergillosis scaled to a mouse lung, the experimental system used in this study, focusing on the "battle over iron" between host and fungus. It integrates the critical players in the early immune response and the known mechanisms that govern their behavior and interactions. It is divided into six conceptual components: space and time, molecules, host cells, *Aspergillus fumigatus*, interactions between different cells, and cells and molecules, and iron metabolism, as briefly described here.

Space and time

A three-dimensional space representing a small portion of a mouse lung is divided into a discrete grid of one thousand voxels (10 voxels in each of 3 dimensions), representing a total volume of 6.4×10^{-2} μL. Each voxel has an edge length of 40 μm ($6.4 \times 10^{-5} \mu L$). Cells and molecules have no space coordinates other than the voxel in which they are located at a given time. This approach is similar to that used in the general immune modeling platform C-IMMSIM [13]. The space has periodic boundary conditions, and simulated time progresses in discrete steps of two minutes.

Molecules

The model includes five kinds of molecules: cytokines (IL6, IL10, TGF, TNF, CXCL2, CCL4), a siderophore (TAFC), iron carrier molecules (transferrin and lactoferrin), iron, and the hormone hepcidin. The cytokines are subject to a half-life of one hour [14–20]. Furthermore, all the molecules are subject to a constant exchange between the simulated volume and the serum (system). Iron in this model is used only as a temporary buffer for the transference of iron between dying cells (i.e., macrophages, *A. fumigatus*) and iron-carrier molecules.

The concentration of a molecule in one voxel is called the local concentration, and we will refer to the concentration across the whole simulated space as the global concentration. In contrast, the serum concentration (i.e., outside the simulator) is the systemic concentration. Equation 1 determines the flux

of molecules between the serum and the simulated (local) space. For the cytokines lactoferrin and TAFC, we assume as a simplification that the systemic concentration x_{system} is zero. Therefore, these molecules are constantly flowing in the direction of the serum, increasing their decay rate. The systemic level of hepcidin and transferrin is dynamically calculated as follows:

$$y = (x - x_{system}) \times e^{-k_{turn} \times t} - x_{system}, \tag{1}$$

where x_{system} is the molecule's systemic concentration (see terminology above), x is the local concentration, k_{turn} is the turnover rate, and t is the time-step length (2 min).

Equations 2 and 3 compute the systemic levels of hepcidin and transferrin. Note that the result of the first equation (2) feeds into the second one (3). However, the first equation needs the systemic levels of IL6 as input. However, in this simulator, we only have the local and global levels of IL6. According to Goncalves, SM *et al.* 2017 [21], a reasonable estimate of the systemic level of IL6 is one-half of its global level. The equations are:

$$Log_{10}(Hepcidin_{systemic}) = hep_{int} + hep_{slope} \times Log_{10}(\frac{IL6_{global}}{2}), \tag{2}$$

$$Ttransferrin_{systemic} = Tf_{int} + Tf_{slope} \times Log_{10}(Hepcidin_{systemic}). \tag{3}$$

These equations are based on data from Tabbah S *et al.* 2018 [22], correlating systemic levels of IL-6 to systemic levels of hepcidin, and Moran-Lev H *et al.* 2018 [23] correlating transferrin and hepcidin. To ensure biologically meaningful values we only evaluate these equations if $IL6_{global} > 1.37 \times 10^{-10} M$, and $Hepcidin_{systemic} > 10^{-8} M$.

All these molecules, except iron, diffuse through space, modeled using the Alternating Direction Implicit (ADI) method with a periodic boundary condition [24]. The rationale for periodic boundary conditions is that the simulation covers a small area amid a large infected area. Therefore, the concentration of molecules across the boundaries should be similar.

Host Cells

There are three types of host cells: type II pneumocytes, macrophages, and neutrophils. The host cells can assume several different states and transition from one to another upon interacting with other agents or molecules. Figure 1 shows the graph of host cell states. We introduce the states "activating" and "inactivating" to model the delay between signal and phenotype change. For a review of macrophage activation/inactivation, see Duque, GA & Descoteaux, A 2014 [25] and Gordon, S 2003 [26].

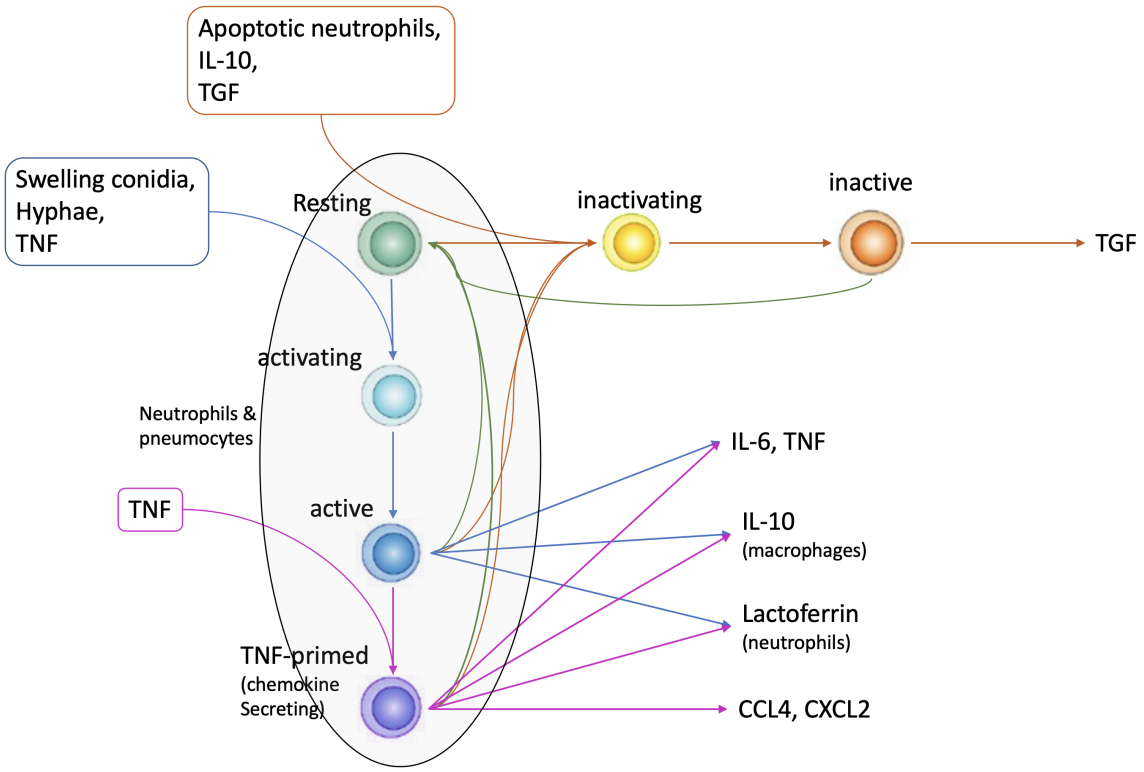

Fig 1. Figure showing host cells state changes. The paragon host cells in the model are the macrophages. Therefore, this figure represents the whole state space of a macrophage. The other cells (neutrophils and type II pneumocytes) have a subset of the states macrophages have (see the area in the ellipses). By default, host cells are in a resting state. Swelling conidia, hyphae, or TNF causes them to transition to an activating (intermediate) state and then to the active state. Active host cells secrete TNF, IL-6, and IL-10. Extra priming with TNF makes host cells secrete chemokines as well (CCL4 and CXCL2). All macrophages return to a resting state after 6 hours (180 iterations) in the absence of a continuous stimulus. Apoptotic neutrophils, IL-10, or TGF-β, cause macrophages (including activated macrophages) to transition to an anti-inflammatory TGF-β-secreting state. Active macrophages (blue and purple) can kill hyphae whereas resting and anti-inflammatory ones cannot.

Leukocytes are free to move through the space and can be recruited as well. Recruitment is done according to Equation 4:

$$n = \frac{k_r \times X}{k_d} \times (1 - \frac{N}{K}), \tag{4}$$

where N is the current number of cells in the simulator, K is the carrying capacity, k_r is the global recruitment rate, k_d is the dissociation constant of the chemokine, X is the global amount of the chemokine (*i.e.*, the average concentration of chemokine in the simulator), and n is the average number of cells to be recruited. This number is used by a Poisson random number generator to decide how many cells will be recruited. Macrophages and neutrophils have half-lives of 24 and 6 hours, respectively [27, 28]. The quantity of cells in the simulator is a balance between the number of cells recruited according to Equation 4 and the number of cells that die. Macrophages are recruited by CCL4 and neutrophils by CXCL2.

In the absence of chemokines, cells move randomly, while in their presence, they tend to move to the voxels with higher chemokine concentrations. The rate of movement is constant, and the cells will, on average, traverse a fixed number of voxels per time step. In the presence of chemokines, each voxel receives a weight according to Equation 5:

$$w_i = 1 - e^{-\frac{x_i}{k_d}}, \tag{5}$$

where x_i is the chemokine concentration in neighboring voxel i, w_i is the corresponding weight of this voxel, and k_d is the chemokine dissociation constant. The cell will then move to a neighboring voxel (v_i) with probability proportional to the voxel weight ($p_i \propto w_i$).

Aspergillus

In the model, *Aspergillus fumigatus* has three life stages: resting conidia, swelling conidia, and hyphae. The hyphae are more or less continuous structures divided by septae [29]. Each of these subdivisions is a multinucleated cell-like structure, referred to as a hyphal cell for simplicity.

In previous work, a dynamic gene regulatory network of iron uptake by *Aspergillus fumigatus* was developed [12], in the form of a Boolean network, that is used here as a component model, with minor adjustments. While the original network had a TAFC node activating the node LIP, the labile iron pool, representing metabolically available iron, we modified it as follows. Instead, when TAFC is activated, the cell secretes TAFC. Later on, if the cell is expressing the siderophore receptors, the cell takes up TAFCBI (TAFC Bound to Iron) from the environment. The TAFCBI uptake increases the cell's total iron pool. The LIP node then becomes a function of the iron pool. Using Equation 6, we activate LIP if the iron pool is high. Resting conidia do not produce or take up TAFC in our model. We update the Boolean network every 30 minutes (every 15 iterations of the tissue-scale model) [30].

In simulations, *Aspergillus fumigatus* starts out as a pool of resting conidia; after 4 hours these start swelling with a half-life of 6 hours (see Table S1) - that is, half the conidia swell after 6h. Beyond that, it takes 2 hours until they become able to grow into hyphal cells. However, growth is controlled by LIP. That is, if LIP is off, hyphae cannot develop, consistent with the known importance of iron for hyphal growth.

Although hyphal growth is a continuous process, the model uses a discrete approximation. A tip cell can produce another tip cell (elongation), while a sub-tip cell can form a 45-degree branch (subapical branch) [29, 31] with a 25% probability. Other cells cannot originate new cells unless their neighbors are killed, and they become tip or sub-tip cells again.

Interactions

Table S2 displays the interactions between all cell types and molecular species. Note that cells/agents may interact with each other in more than one way, depending on their state. For example, the agent "Afumigatus" (that represents *Aspergillus fumigatus*) has the states "resting conidia," "swelling conidia," and "hyphae." The interaction between this agent and a neutrophil will be different depending on this state (see Table S2). Due to software engineering considerations, we consider the secretion of molecules a kind of interaction between a cell and a molecule. Therefore, interactions between molecules and cells can also be of two kinds: receptor binding (interaction in the biological sense) and secretion. Note that, in Table S2, macrophages need to be active in order to interact with hyphae, while neutrophils do not. For agents to interact with each other, they must be in physical proximity, *i.e.*, in the same voxel.

Interactions between cells and molecules follow Equation 6:

$$p = 1 - e^{-\frac{x}{k_d}}, \tag{6}$$

where x is the molecule concentration, k_d is its dissociation constant, and p is the probability of receptor activation. Likewise, interactions between molecules (i.e., reactions) follow the Michaelian equation (Equation 7):

$$v = \frac{K_{cat} \times S1 \times S2}{K_M + S1}. \tag{7}$$

Scaling from the simulated space to the whole mouse lung

A pair of mouse lungs is assumed to have a volume of 1mL [32], containing 2.3×10^5 macrophages in the alveolar lumen [33] and 1×10^7 type-II alveolar epithelial cells [34]. The simulated space is $6.4 \times 10^{-2} \mu L$, thus containing 15 macrophages and 640 type-II epithelial cells initially. A high dose inoculum (10^7) is used for initialization. However, according to Pritchard, JN *et al.* 1985 [35], inoculated material distributes unevenly, with $\approx 1/3$ of the lung infected and the remainder clear. Scaling appropriately, the simulated space should have 1920 conidia. To scale neutrophils, one can also use the fact that infection is limited to $\approx 1/3$ of the lung. In other words, to convert the number of neutrophils and fungal spores in the simulated space to the whole lung number, one needs to multiply by 5028.

Experimental methods

Neutrophil depletion and induction of aspergillosis.

All experiments were performed in accordance with the National Institutes of Health and Institutional Animal Care and Use Guidelines and were approved by the Animal Care and Use Committee of the University of Florida. Eight week-old male and female C57Bl/6 mice were purchased from the Jackson Laboratory and housed under specific pathogen-free conditions in the animal facilities of the University of Florida, and infected with Aspergillus as previously described by us [36]. Briefly, neutrophils were transiently depleted with an intraperitoneal injection of $400\mu g$ of anti-Ly6G antibody (clone 1A8, BioXcell) in 0.5ml saline. A cohort of mice received an equivalent amount of isotype control antibody (rat IgG2a, Clone 2A3, BioXcell), a day prior to intratracheal inoculation with 7×10^6 *Aspergillus* conidia.

Flow Cytometry

Mouse lung flow cytometry was performed as described in [37]. Briefly, lungs were digested in a mixture of 200 $\mu g/mL$ DNaseI and 25 $\mu g/mL$ Liberase TM for 30 mins at 370 $°C$. The digested lungs were serially passed through 70 and 40 μm filters to collect the single-cell suspension. After red blood cell lysis, cells were counted, and 1.5×10^6 cells were stained with a fixable APC Cy-7 conjugated live dead stain (Thermo Fisher) in PBS for 20 mins. After washing with FAC buffer, cells were incubated with anti-CD16/32 (Fc block, clone 93; eBioscience, San Diego, CA) and stained with PerCP-conjugated anti-CD45 (30-F11), FITC-conjugated anti-CD11b (M1/70), PE-conjugated CD64 (X54-5/7.1), PECy7-conjugated anti-CD11c (N418), V450-conjugated anti-MHCII (I-A/I-E), APC-conjugated anti-CD24 (M1/69), BV605-conjugated anti-Ly6g (1A8), BV711-conjugated Ly6c (HK 1.4), Texas Red -conjugated Siglec F (E50-2440). Flow cytometry data were acquired using 14 color BD Fortessa (BD Biosciences, San Jose, CA). 500,000 events /samples were acquired and analyzed with FlowJo software 9.0 (Tree Star Inc., Ashland, OR).

Bronchoalveolar lavage fluid cytokine measurement

BALF IL-6 and CXCL2 levels were measured using commercial ELISA kits (Invitrogen), as per manufacturers' instructions.

Results

Model validation

This model was completely parameterized with data from the literature (see Supplementary Materials), thereby assuring a much broader validity than could be obtained through parameter fitting to a small collection of experimental time-course measurements. We have validated the model in two ways. Firstly, we show that it provides a good qualitative fit with several time-course data sets in the literature that were not used in model calibration. We used a collection of papers that report time-series of critical variables present in the model, such as neutrophils, TNF, IL6, and colony-forming units (CFU). These

values are compared with those predicted by model simulation. These data are used to test if the model can reproduce the reported levels of the different variables and, most importantly, their timing. None of the papers selected for validation were used to calibrate the model.

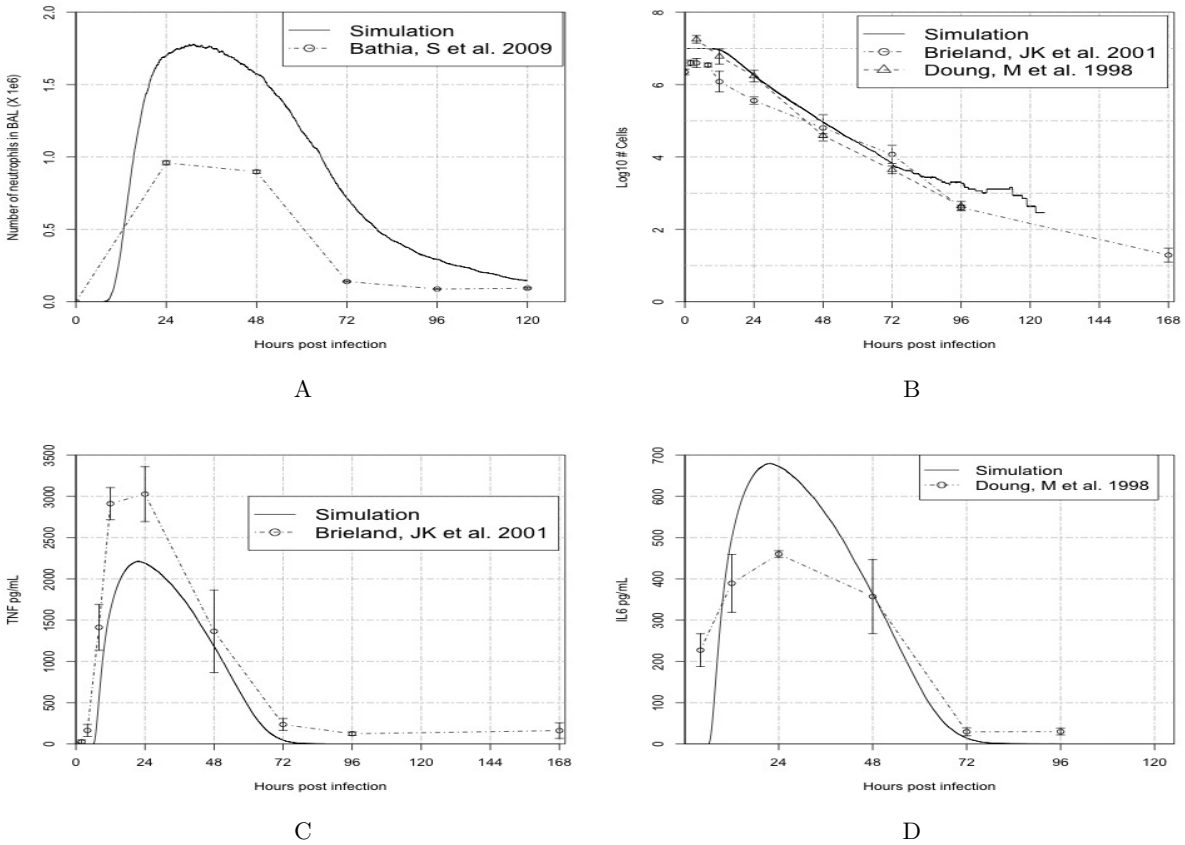

Fig 2. Figure showing the comparison of simulated data with data reported in the literature. To produce this figure, 36 simulations were performed, starting with an average of 1920 conidia, 15 macrophages, and 640 epithelial cells. Figure 2A: simulated time series of neutrophils and a time series reported by Bhatia, S *et al.* 2011 [38]. Figure 2B: simulated time series of conidia and time series reported by Brieland, JK et al. 2001 [39] and Doung, M *et al.* 1998 [40]. Figure 2C: simulated time series of TNF and time series reported by Brieland, JK *et al.* 2001 [39]. Figure 2D: simulated time series of IL-6 and time series reported by Doung, M *et al.* 1998 [40].

Figure 2 exhibits the comparison of simulation results with literature data. One can observe that the simulator correctly captures the timing of cell counts and cytokine levels. Furthermore, CFU dynamics (Figure 2B) is also accurately captured by the model. Concerning the exact levels of these cells and cytokines, the mismatches between our simulator and the data in Figure 2 are within the range of variation between the different experiments reported in the literature (Table 1). Figure 3 shows that our model correctly predicts the fall in CXCL2 upon injection of anti-TNF-α.

Next, we compared model simulations with a published experiment of mice injected with anti-TNF-α. This cytokine is one of the critical drivers of the immune response and one of the key molecules inducing the secretion of chemokines. In Mehrad et al. 1999 [41], the level of chemokines fell 24 hours post-infection upon injection with an anti-TNF antibody. To reproduce this experiment, we estimated the affinity of an antibody for a protein antigen with data from the literature [42]. Note that those estimates are for a generic protein antigen and not for TNF specifically.

We did an extensive literature search for data concerning *Aspergillus fumigatus* infection in mice. We

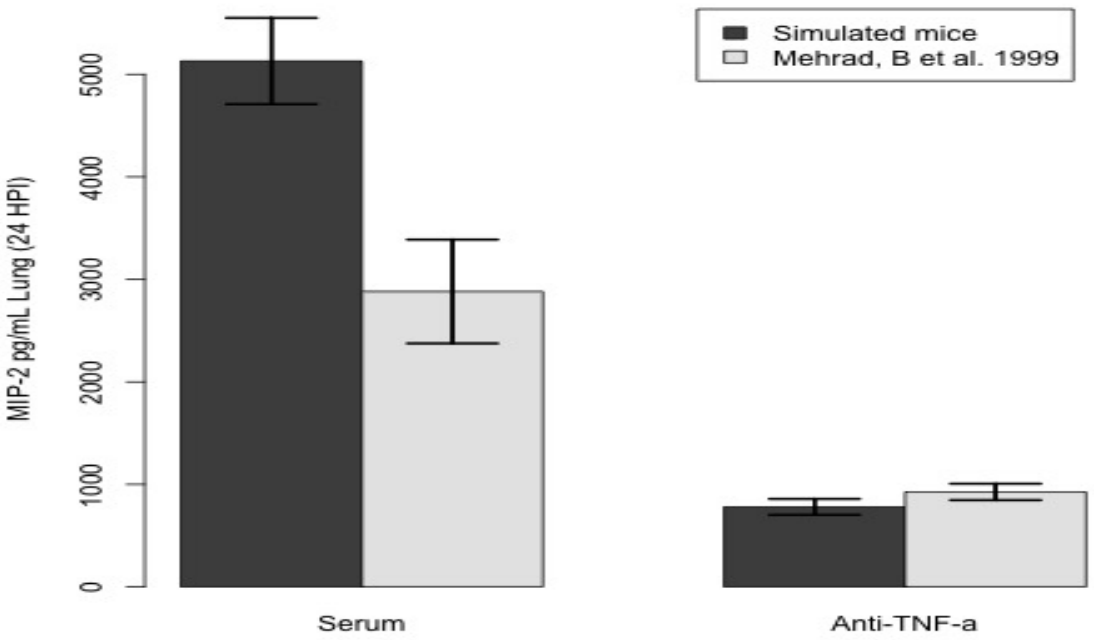

Fig 3. Figure showing the comparison of simulated data with data reported by Mehrad, B *et al.* 1999 [41]. Mice were injected with serum or antibody (anti-TNF) concentration of 2×10^{-8} M, reaction rate 1.72×10^{8} $M * s^{-1}$ (Kcat/Km), and half-life of 5 days, 24 before infection. To produce this figure, 36 simulations were performed, initialized with an average of 1920 conidia, 15 macrophages, and 640 epithelial cells.

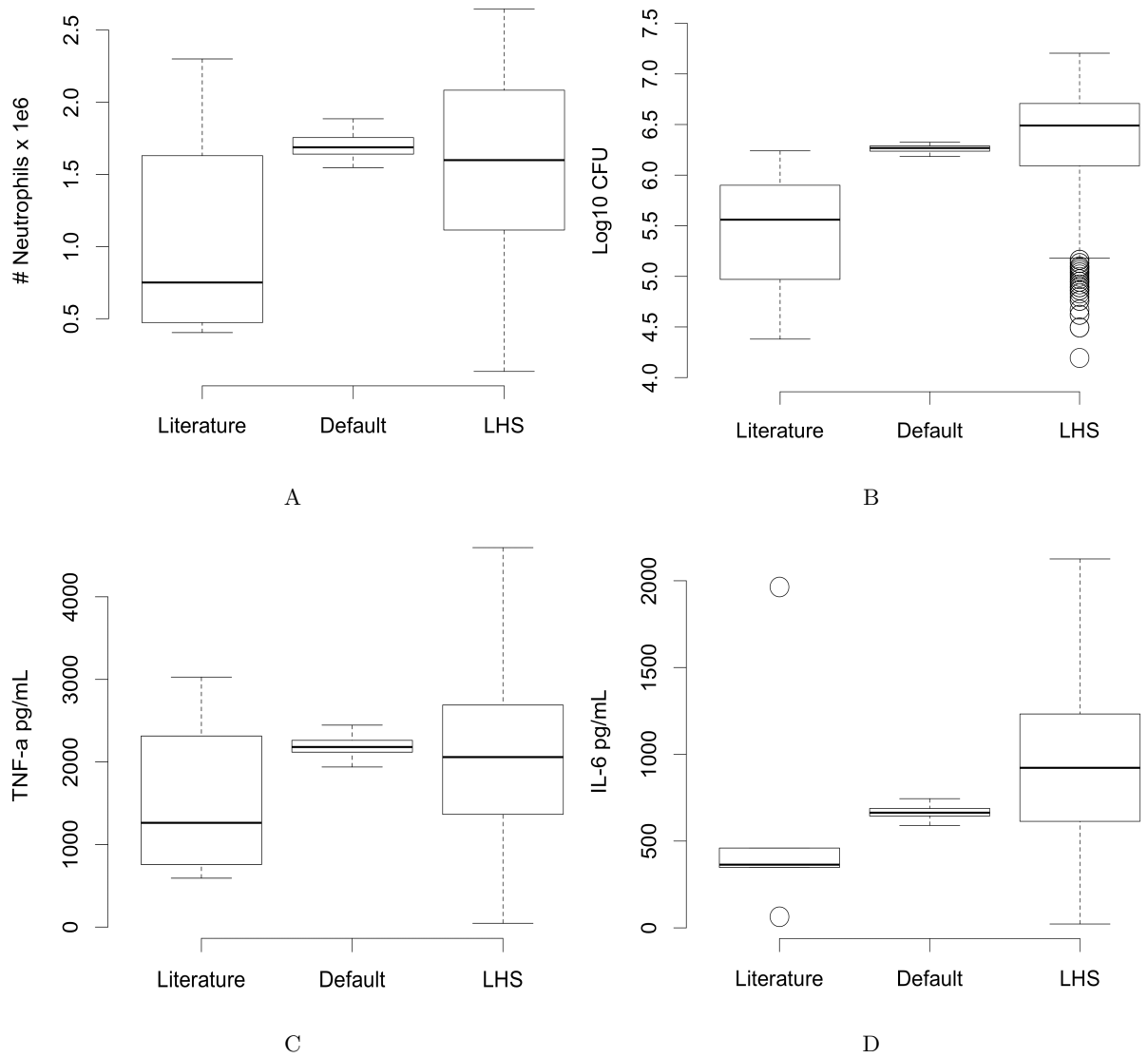

Fig 4. Figures showing the comparison of simulated data with extended literature reported data (Table 1). Literature: data from the literature (Table 1). Default: simulator run with default values. LHS simulator run with parameters sampled with LHS. To generate the "Default," we run 36 simulations with the default parameter values of the simulator; see Supplementary Table S1. To generate the "LHS," we run 1200 simulations with LHS sampled around the default values.

Table 1. Table showing extended literature measurements of *Aspergillus fumigatus* outcome parameters. All the papers in this table report data in BAL upon 24 hours post-infection and inoculate mice with $\approx 10^7$ conidia. Column 1 shows the reference; column 2 reported measurements of TNF; column 3 IL-6; column 4 neutrophils; and column 5 log_{10} of CFU.

Reference	TNF	IL-6	Neutrophils	$Log_{10}(CFU)$
Bhatia, S *et al.* 2011 [38]			$9.60 \pm 0.14 \times 10^5$	
Brieland, JK *et al.* 2001 [39]	$3027 \pm 194 pg/mL$			5.56 ± 0.10
Cenci, E *et al.* 2001 [43]	$1602 \pm 297 pg/mL$	$348 \pm 52 pg/mL$		
Dubourdeau, M *et al.* [44]	$923 \pm 174 pg/mL$	$64 \pm 18 pg/mL$		
Doung, M *et al.* 1998 [40]		$460 \pm 8 pg/mL$		6.24 ± 0.16
Gresnigt, MS *et al.* 2016 [45]		$364 \pm 47 pg/mL$	$5.42 \pm 1.64 \times 10^5$	
Hohl, TM *et al.* 2005 [46]			$2.30 \pm 0.92 \times 10^6$	
Teschner, D *et al.* 2019 [47]	$592 \pm 48 pg/mL$	1964 ± 313	$4.04 \pm 1.25 \times 10^5$	4.38 ± 0.38
Average ± std-dev	**1536±1079 pg/mL**	**676 ± 748 pg/mL**	$\mathbf{1.05 \pm 0.87 \times 10^6}$	$\mathbf{5.39 \pm 0.94}$

compiled this data in Table 1. It represents BAL measurements of IL-6, TNF, CFU, and neutrophils 24 hours post-infection with 10^7 conidia. One can observe that these data have significant variability. To understand how our simulated data compare to these measurements, we sampled parameters with Latin Hypercube Sampling (LHS) and ran 1200 simulations. Figure 4 displays the comparison between several literature measurements, the simulator with the default parameters (Table S1), and the simulator with LHS parameters. The predictions made by our simulator are within the range of variation between data reported in the literature. Note that the simulator can also reproduce the variability in biological data. This variability is due to differences in hosts, different fungal strains, and experimental conditions. These conditions sometimes generate different but qualitatively equivalent outcomes. Our simulator is robust to a wide range of parameters, with variability similar to that observed in the literature Figure; see 4.

In vivo validation of simulation results

As discussed above, due to the high variability in experimental design (fungal dose, techniques of infection, etc.) and in the measurements summarized in Table 1, we decided to further validate the model results, in particular the ability of the simulator to reproduce temporal dynamics, with an *in vivo* experimental design that most closely resembles the simulator setup. We infected immunocompetent mice with 7×10^6 conidia intratracheally and measured cytokines and leukocytes from 0-72 hours post-infection (see description in the Experimental Methods section). Figure 5 shows that our simulator can correctly predict the timing of the immune response, as indicated by levels of IL-6, neutrophils, macrophages, and CXCL2.

Figure 5 shows remarkable agreement between the timing of cytokines and cells measured by our own experiments and the dynamics produced by the simulator. To recall, ABMs are not continuous-time models, since they advance in discrete time steps. The actual time these steps correspond to is estimated by considering the events that take place from one time step to the next. In our case, we estimated that our time steps correspond to two minutes of simulated time. Thus, the agreement in timing is a key step in validating model predictions, since the timing of events in the immune response to this infection is crucial for infection outcome and determination of interventions.

Identification of drivers of fungal burden

In order to demonstrate the usefulness of the model as a discovery tool for new immunological insights, we use it to investigate the significance of the different mechanisms for fungal growth over time, by measuring their effect on the maximal fungal burden encountered over a 24 hour time span. For this purpose, we conducted the following simulation experiment. Using Latin Hypercube Sampling, as before, we chose 1200 parameter sets. For each of these, we carried out simulation runs with both immunocompetent and neutropenic hosts and counted the number of live hyphal cells over a 24 hour time period. The maximum number encountered during this simulation run was reported as "fungal

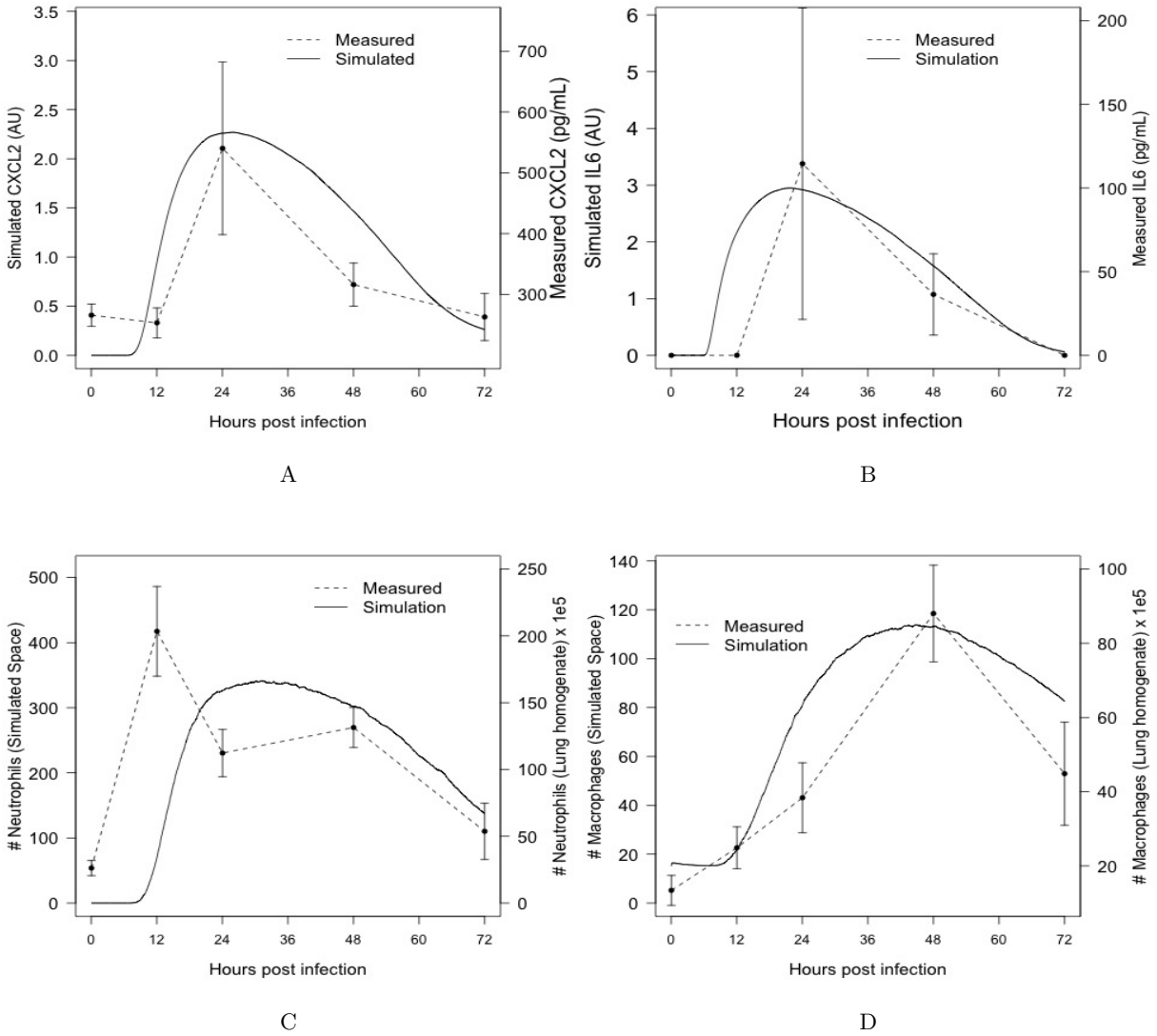

Fig 5. Figure showing the comparison of our experimental data on immunocompetent mice with simulation results. For this purpose, 36 simulations were performed, starting with an average of 1920 conidia, 15 macrophages, and 640 epithelial cells. Figure 5A: Comparison of simulated time series of CXCL2 with experimental data measured in BAL. Figure 5B: Comparison of simulated time series of IL-6 with experimental data measured in BAL. Figure 5C: Comparison of the number of neutrophils in the simulated space with the number of neutrophils in lung homogenate. Figure 5D: Comparison of the number of macrophages/monocytes in simulated space with the number of monocytes in lung homogenate. Experimental data refer to mice infected with 7×10^6 conidia.

Table 2. Table summarizing the classification results from Figures S2 and S3. The table shows qualitatively the groups of parameters that lead to the extremes of high and low germination and hyphal proliferation over 24 hours of simulated time. Intermediate conditions are not presented here. The plus and minus signs represent, qualitatively, the classifications. For example, in column 4 (immunocompetent, high burden), the three plus signs and one minus sign indicate that the corresponding partition tree (Figures S2) partitioned the data set by the fungal growth rate, activation rate, swelling rate, and recruitment rate, and selected the upper part of the first three partitions (plus sign) and the lower part of the last (minus sign). In a qualitative sense, this means that that class (immunocompetent, high burden) is associated with high growth rate, activation rate, and swelling rate, and with low recruitment rate. The partitioning hierarchy is not represented in this table, as it is meant to be simply a general summary. Some of the parameters shown in the table do not contribute to the extreme cases reported here; they are kept for completeness. These parameters, however, play a role in differentiating intermediate cases of fungal burden (Figures S2 and S3).

Parameters	**Parameter Description**	**Immunocompetent**		**Neutropenic**	
		Low Burden	**High Burden**	**Low Burden**	**High Burden**
GR_RT	growth rate	-	+	-	+
ITER_CH_ST	iterations needed to host cells chance state		+		+
MV_RT	leukocytes moviment rate				
REC_RT	leukocytes recruitment rate		-		-
PR_SW	probability of conidia swelling		+		+
TAFC_QTTY	TAFC secretion rate				+
ITER_GER	Iterations swelling conidia takes to starts germinating				
PR_BR	Probability of hyphae branching				
Max # hyphae		**28**	**1609**	**133**	**5203**
Max # hyphae / Intial inoculum		**1.5%**	**83.79%**	**6.9%**	**271%**

burden." (Note that after initial uninhibited growth, the immune response may cause a subsequent drop in the number of live hyphal cells.)

We carried out a classification of parameters and their influence on fungal growth rate, encoded by a collection of classification trees in Figures S2 and S3 in the Supplementary Materials. The results are summarized in Table 2.

Our analysis shows that eight model parameters are most strongly correlated to fungal burden. As would be expected, the most critical parameter is the intrinsic growth propensity of a given fungal strain to grow, (GR_RT), that remains fixed for a given fungal strain [48]. Fixing this parameter, we then asked which other parameters were associated with high, respectively low, fungal burden over a 24-hour period. To do this, we measured the variation of the square of the correlation r^2 between the model parameters and fungal burden as the growth rate increases. Figure 6 shows the variation of r^2 for the seven most important parameters (not including intrinsic growth rate) indicated by our analysis in Table 2.

Figure 6 shows that, as the intrinsic growth rate of the fungus increases, the relative importance of the seven other parameters changes. As an example, Figure 6D shows that when the fungal growth rate is very high or very low, the leukocyte movement rate is weakly correlated with fungal burden. However, this parameter is critical in determining the actual fungal burden in strains with an intrinsic growth rate near the default 29 $\mu m/h$ (Table S1). The leukocyte movement rate is an intrinsic feature of the immune system. However, according to Figure 6D, this feature is more or less critical, depending on the virulence of the strain, being most important for a moderately virulent strain ($21 - 28\mu m/h$). This might explain some of the variance in the course of the infection between hosts.

Figure 6 shows that overall the seven parameters tend to be more critical when the intrinsic growth rate is close to its default value. That is, their importance wanes as the growth rate becomes very high or very low. However, the importance of the swelling rate, measured as the average number of time steps needed for conidia to germinate, and the average time to immune cell activation have a bias towards a high growth rate (Figure 6A, B, and D). On the other hand, the TAFC secretion rate has a bias towards a low growth rate (Figure 6C). Finally, the monocyte recruitment rate is not sensitive to intrinsic growth rate variation (Figure S4C).

The results in Figure 6 also show that activation, germination, and recruitment rates have a bigger influence in immunocompetent hosts (Figure 6B, D, and Figure S4C). Meanwhile, swelling rate, TAFC secretion rate, and branching probability are more crucial in neutropenic hosts (Figure 6A, C, and Figure S4A). Finally, the leucocyte movement rate is approximately equally important in neutropenic and immunocompetent hosts (Figure 6D).

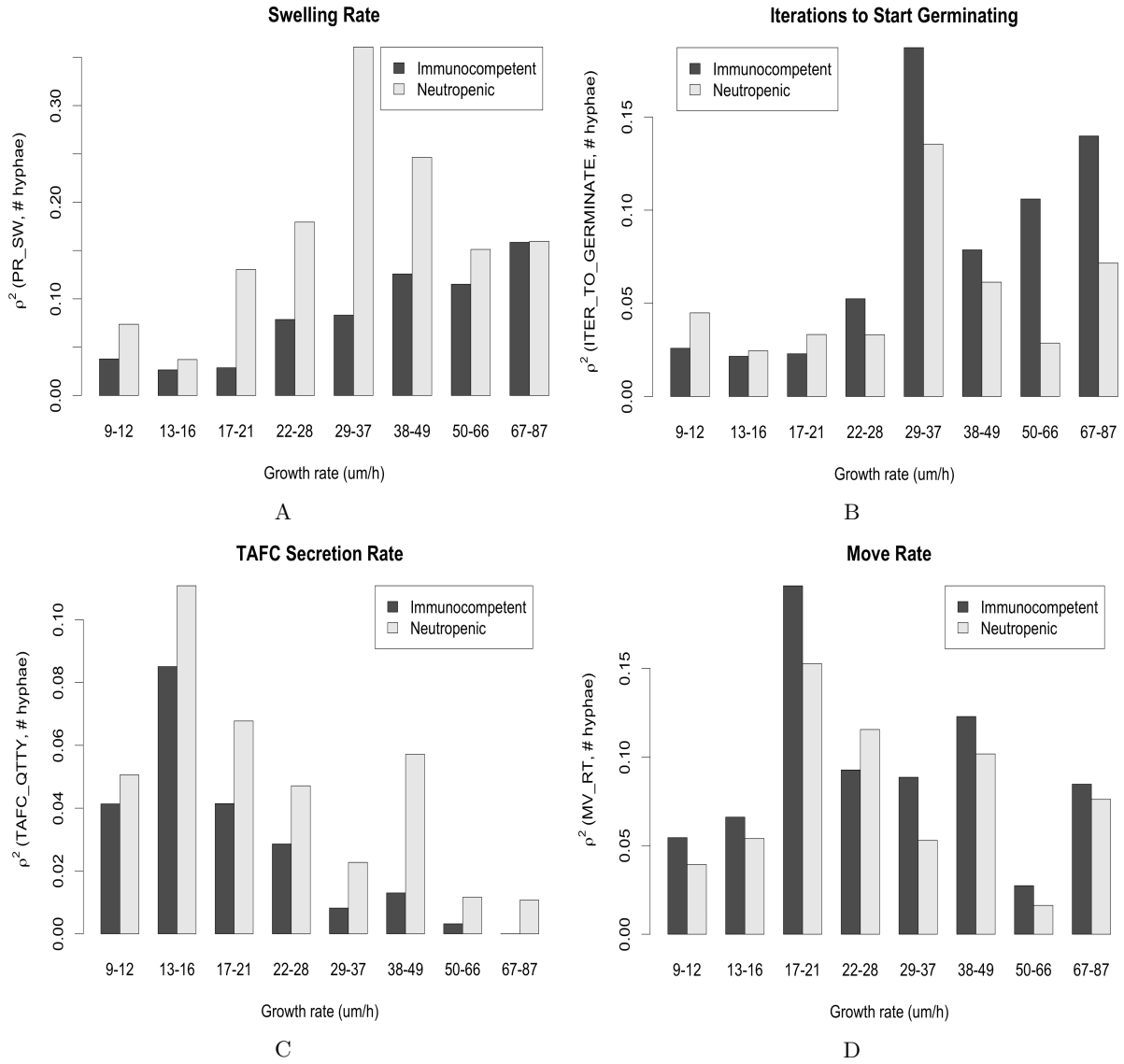

Fig 6. Variation of the square of the correlation r^2 between the critical model parameters and fungal burden, with the variation of the growth rate. We started with a dataset of 1200 samples generated with LHS and then partitioned this dataset by growth rate. The x-axis shows the range of the growth rate in each partition. We then calculate the correlation between parameters and fungal burden in each partition. Fungal burden was measured as the maximum number of hyphal cells measured over the course of 24 hours of simulation. A: Variation of r^2 between the swelling rate and fungal burden. B: Variation of r^2 between germination rate and fungal burden. C: Variation of r^2 between the TAFC secretion rate and fungal burden. D: Variation of r^2 between the leukocyte movement rate and fungal burden.

Discussion

Understanding the innate immune response to pathogens is of the utmost importance for designing effective therapeutic interventions. With the increasing resistance of pathogens to anti-microbial drugs, it is imperative to explore host-centric therapeutics. This is the motivation for the work presented here. The goal was to understand some of the primary components of the innate immune response to fungal pathogens. In order to limit the immense complexity of mechanisms involved, the computational model

presented here is focused on an essential component of nutritional immunity, the "battle over iron" between the host and the fungus in the context of a respiratory infection. The component of the immune response considered here involves many players, ranging from immune and fungal cells to molecular species such as cytokines, iron, and chemokines. It integrates events at the intracellular, tissue, organ, and system levels and is governed by several intertwined feedback loops that create complex dynamics.

Without a computational model that captures relevant biology and is parameterized in a way that makes it more broadly valid and credible, it would be challenging to understand the interplay between the different components and make predictions about the effect of various perturbations. This paper describes a model that satisfies these criteria and can serve as the basis for future investigations. It is one of the most comprehensive models of this infection, parameterized entirely with information from the literature, and is validated using experimental data specifically generated for this purpose. It is also shown that it is broadly valid by verifying that it reproduces a wide range of experimental data reported in the literature (and not used for model calibration). This approach is different from the commonly used method of fitting the model parameters to one or more time courses of experimental data.

As an important application of the model to understanding key features of respiratory fungal infections, we used it to study the importance of model parameters to fungal burden, an important metric for disease progression. The model predicts that different characteristics of the immune system take on different significance in controlling fungal burden, depending on the virulence of the fungal strain in question. However, other factors can also significantly influence fungal burden, such as the siderophore secretion rate and certain aspects of the immune response. These factors also have different degrees of importance, depending on the intrinsic growth rate of the fungal strain.

It was pointed out in Schrettl M et al. 2004 [49] that TAFC is a critical virulence factor. Likewise, in subsequent work, Schrettl M et al. 2007 [50] show that an *Aspergillus* knockout strain without intra- and extracellular siderophores has completely attenuated virulence. Figure 6C shows that the TAFC secretion rate is more important when the growth rate is low. In this case, fewer cells are secreting this siderophore. Consequently, the TAFC concentration becomes a bottleneck. In fact, our analysis shows that the concentration of TAFC bound to iron in neutropenic hosts with a high growth rate is 60% higher than in simulations with a low growth rate (result not shown). For immunocompetent hosts, a smaller and less significant difference was observed.

Interestingly, the classification trees (Figure S3, Table 2) show that a high TAFC secretion rate is also necessary for achieving high fungal burden. However, in this case, the TAFC secretion rate acts only in synergy with other parameters. Inhibiting TAFC secretion alone, nevertheless, can break the synergy and reduce fungal burden.

Conidial swelling is the first step to germination and subsequent hyphal growth. However, this is also the time when the fungus become visible to the immune system. Therefore, there are two competing forces upon swelling. The fact that swelling is a necessary step before growth is advantageous for the fungus. This is evidenced by the positive correlation between the swelling rate and fungal burden (results not shown). However, the fact that swelling makes the conidia visible to the immune system and that conidia are easier to kill than hyphae creates a disadvantage for the fungus. This is evidenced by the bias towards a high growth rate (Figure 6A) in this case. That means that swelling is more advantageous if, upon swelling, hyphae develop quickly. A recent model published by Ewald, J *el al.* 2021 [51] came to similar conclusions.

Interestingly, the parameter ITER_GER that controls the time conidia take to germinate after swelling - with two hours being the default value [50] - has a negative correlation with growth rate (result not shown). This negative correlation reinforces that conidia become susceptible to the immune system and need to germinate rapidly upon swelling.

The ability of leucocytes to locate fungal cells is crucial for controlling the infection [9, 11]. The factors that affect it are chemotaxis and movement rate. Figure 6D shows that the leukocyte movement rate is one of the most prominent parameters to control fungal burden with r^2 around 0.2 when the growth rate is in the range 21-28 $\mu m/h$. However, our analysis also indicates saturation. When the growth rate is too high, the immune system is overwhelmed by fungal growth. Conversely, if the growth rate is too low, the immune system quickly gains the upper hand.

Availability of code and data

The model code and all experimental data used for model validation are available in the Github repository https://github.com/NutritionalLungImmunity/IPA_model

Supporting information

S1 File. Contains supplementary information on many aspects of the model, model parameters, and simulation.

Acknowledgments

This work was supported by the following grants: NIH 1U01EB024501-01, NSF CBET-1750183, and NIH 1 R01AI135128-01. R.L. was also partially supported by NIH Grant 1R01GM127909-01, B.M. by American Heart Association Grant 18TPA34170486, and B.A. by NIH Grant NIH T90-DE021989.

References

1. Pappas P, et al. Invasive fungal infections among organ transplant recipients: results of the Transplant-Associated Infection Surveillance Network (TRANSNET). Clin Infect Dis. 2010;50:1101–11.

2. Mitaka H, Kuno T, Takagi H, Patrawalla P. Incidence and mortality of COVID-19-associated pulmonary aspergillosis: A systematic review and meta-analysis. Mycoses. 2021;64(9):993–1001. doi:https://doi.org/10.1111/myc.13292.

3. Chong W, Neu K. Incidence, diagnosis and outcomes of COVID-19-associated pulmonary aspergillosis (CAPA): a systematic review. J Hosp Infect. 2021;113:115–129. doi:10.1016/j.jhin.2021.04.012.

4. Neofytus ea D. Epidemiology, outcomes, and mortality predictors of invasive mold infections among transplant recipients: a 10-year, single-center experience. Transpl Infect Dis. 2013;15:233–242.

5. van der Linden J, et al. Aspergillosis due to voriconazole highly resistant Aspergillus fumigatus and recovery of genetically related resistant isolates from domiciles. Clin Infect Dis. 2013;57:513–520.

6. Denning D, et al. Global burden of chronic pulmonary aspergillosis as a sequel to pulmonary tuberculosis. Bull World Health Organ. 2011;89(12):864–72.

7. Ganz T. Iron and infection. Int J Hematol. 2018;107(1):7–15. doi:10.1007/s12185-017-2366-2.

8. Blatzer M, Latge J. Metal-homeostasis in the pathobiology of the opportunistic human fungal pathogen Aspergillus fumigatus. Curr Opin Microbiol. 2017;40:152–159. doi:10.1016/j.mib.2017.11.015.

9. Pollmächer J, Figge MT. Agent-based model of human alveoli predicts chemotactic signaling by epithelial cells during early Aspergillus fumigatus infection. PloS one. 2014;9(10):e111630.

10. Pollmächer J, Figge MT. Deciphering chemokine properties by a hybrid agent-based model of Aspergillus fumigatus infection in human alveoli. Frontiers in microbiology. 2015;6:503.

11. Oremland M, Michels KR, Bettina AM, Lawrence C, Mehrad B, Laubenbacher R. A computational model of invasive aspergillosis in the lung and the role of iron. BMC systems biology. 2016;10(1):1–14.

12. Brandon M, Howard B, Lawrence C, Laubenbacher R. Iron acquisition and oxidative stress response in Aspergillus fumigatus. BMC systems biology. 2015;9(1):19.

13. Castiglione F. In: Meyers RA, editor. Agent Based Modeling and Simulation, Introduction to. New York, NY: Springer New York; 2009. p. 197–200.

14. Huhn RD, Radwanski E, Gallo J, Affrime MB, Sabo R, Gonyo G, et al. Pharmacodynamics of subcutaneous recombinant human interleukin-10 in healthy volunteers. Clinical Pharmacology & Therapeutics. 1997;62(2):171–180. doi:https://doi.org/10.1016/S0009-9236(97)90065-5.

15. Zahn G, Greischel A. Pharmacokinetics of tumor necrosis factor alpha after intravenous administration in rats. Dose dependence and influence of tumor necrosis factor beta. Arzneimittelforschung. 1989;39(9):1180–1182.

16. Oliver J, Bland L, Oettinger C, Arduino M, McAllister S, Aguero S, et al. Cytokine kinetics in an in vitro whole blood model following an endotoxin challenge. Lymphokine Cytokine Res. 1993;12(2):115–120.

17. Kuribayashi T. Elimination half-lives of interleukin-6 and cytokine-induced neutrophil chemoattractant-1 synthesized in response to inflammatory stimulation in rats. Lab Anim Res. 2018;34:80–83. doi:https://doi.org/10.5625/lar.2018.34.2.80.

18. Castell JV, Geiger T, Gross V, Andus T, Walter E, Hirano T, et al. Plasma clearance, organ distribution and target cells of interleukin-6/hepatocyte-stimulating factor in the rat. European Journal of Biochemistry. 1988;177(2):357–361. doi:https://doi.org/10.1111/j.1432-1033.1988.tb14383.x.

19. Toft A, Falahati A, Steensberg A. Source and kinetics of interleukin-6 in humans during exercise demonstrated by a minimally invasive model. Eur J Appl Physiol. 2011;111:1351–1359. doi:https://doi.org/10.1007/s00421-010-1755-5.

20. Wakefield L, Winokur T, Hollands R, Christopherson K, Levinson A, Sporn M. Recombinant latent transforming growth factor beta 1 has a longer plasma half-life in rats than active transforming growth factor beta 1, and a different tissue distribution. The Journal of Clinical Investigation. 1990;86(6):1976–1984. doi:10.1172/JCI114932.

21. Goncalves SM, Lagrou K, Rodrigues CS, Campos CF, Bernal-Martinez L, Rodrigues F, et al. Evaluation of Bronchoalveolar Lavage Fluid Cytokines as Biomarkers for Invasive Pulmonary Aspergillosis in At-Risk Patients. Frontiers in Microbiology. 2017;8:2362. doi:10.3389/fmicb.2017.02362.

22. Tabbah S, Buhimschi C, Rodewald-Millen K, Pierson C, Bhandari V, Samuels P, et al. Hepcidin, an Iron Regulatory Hormone of Innate Immunity, is Differentially Expressed in Premature Fetuses with Early-Onset Neonatal Sepsis. Am J Perinatol. 2018;35(9):865–872. doi:10.1055/s-0038-1626711.

23. Moran-Lev H, Weisman Y, Cohen S, Deutsch V, Cipok M, Bondar E, et al. The interrelationship between hepcidin, vitamin D, and anemia in children with acute infectious disease. Pediatr Res. 2018;84(1):62–65. doi:10.1038/s41390-018-0005-0.

24. Chang MJ, Chow LC, Chang WS. Improved Alternating-Direction Implicit Method For Solving Transient Three-Dimensional Heat Diffusion Problems. Numerical Heat Transfer, Part B: Fundamentals. 1991;19(1):69–84. doi:10.1080/10407799108944957.

25. Arango Duque G, Descoteaux A. Macrophage Cytokines: Involvement in Immunity and Infectious Diseases. Frontiers in Immunology. 2014;5:491. doi:10.3389/fimmu.2014.00491.

26. Gordon S. Alternative activation of macrophages. Nat Rev Immunol. 2003;3:23–35. doi:https://doi.org/10.1038/nri978.

27. Patel A, Zhang Y, Fullerton J, Boelen L, Rongvaux A, Maini A, et al. The fate and lifespan of human monocyte subsets in steady state and systemic inflammation. The Journal of experimental medicine. 2017;214. doi:10.1084/jem.20170355.

28. Tak T, Tesselaar K, Pillay J, Borghans JA, Koenderman L. What's your age again? Determination of human neutrophil half-lives revisited. Journal of Leukocyte Biology. 2013;94(4):595–601. doi:https://doi.org/10.1189/jlb.1112571.

29. Maheshwari R. 1. In: Fungi Experimental Methods in Biology. CRC Press; 2005.

30. OJJr T. In: Nuclear Factor Kappa B (NF-kB) Translocation Assay Development and Validation for High Content Screening. NIH; 2012.

31. Riquelme M, Bartnicki-Garcia S. Key differences between lateral and apical branching in hyphae of Neurospora crassa. Fungal Genet Biol. 2004;41(9):842–851. doi:10.1016/j.fgb.2004.04.006. PMID: 15288020.

32. Irvin CG, Bates J. Measuring the lung function in the mouse: the challenge of size. Respiratory research. 2003;4(1). doi:10.1186/rr199.

33. Bonnett CR, Cornish EJ, Harmsen AG, Burritt JB. Early Neutrophil Recruitment and Aggregation in the Murine Lung Inhibit Germination of Aspergillus fumigatus Conidia. Infection and Immunity. 2006;74(12):6528–6539. doi:10.1128/IAI.00909-06.

34. Dzhuraev G, Rodriguez-Castillo J, Ruiz-Camp J, Salwig I, Szibor M, Vadasz I, et al. Estimation of absolute number of alveolar epithelial type 2 cells in mouse lungs: a comparison between stereology and flow cytometry. Journal of Microscopy. 2019;275:36–50. doi:https://doi.org/10.1111/jmi.12800.

35. Pritchard J, Holmes A, Evans J, Evans N, Evans R, Morgan A. The distribution of dust in the rat lung following administration by inhalation and by single intratracheal instillation. Environmental Research. 1985;36(2):268–297. doi:doi.org/10.1016/0013-9351(85)90025-8.

36. Cagnina R, et al. Neutrophil-derived TNF drives fungal acute lung injury in chronic granulomatous disease. J Infect Dis. 2021;doi: 10.1093/infdis/jiab188.

37. Barletta K, et al. Adenosine A(2B) receptor deficiency promotes host defenses against gram-negative bacterial pneumonia. Amer J Respir Crit Care Med. 2012;186(10:1044–50.

38. Bhatia S, Fei M, Yarlagadda M, Qi Z, Akira S, Saijo S, et al. Rapid host defense against Aspergillus fumigatus involves alveolar macrophages with a predominance of alternatively activated phenotype. PLoS One. 2011;6(1):e15943. doi:10.1371/journal.pone.0015943.

39. Brieland J, Jackson C, Menzel F, Loebenberg D, Cacciapuoti A, Halpern J, et al. Cytokine networking in lungs of immunocompetent mice in response to inhaled Aspergillus fumigatus. Infect Immun. 2001;69(3):1554–1560. doi:10.1128/IAI.69.3.1554-1560.2001.

40. Duong M, Ouellet N, Simard M, Bergeron Y, Olivier M, Bergeron M. Kinetic study of host defense and inflammatory response to Aspergillus fumigatus in steroid-induced immunosuppressed mice. J Infect Dis. 1998;178(5):1472–1482. doi:10.1086/314425.

41. Mehrad B, Strieter R, Standiford T. Role of TNF-alpha in pulmonary host defense in murine invasive aspergillosis. J Immunol. 1999;162(3):1633–1640.

42. Goldbaum FA, Cauerhff A, Velikovsky CA, Llera AS, Riottot MM, Poljak RJ. Lack of Significant Differences in Association Rates and Affinities of Antibodies from Short-Term and Long-Term Responses to Hen Egg Lysozyme. The Journal of Immunology. 1999;162(10):6040–6045.

43. Cenci E, Mencacci A, Casagrande A, Mosci P, Bistoni F, Romani L. Impaired antifungal effector activity but not inflammatory cell recruitment in interleukin-6-deficient mice with invasive pulmonary aspergillosis. J Infect Dis. (2001;184(5):610–7. doi:10.1086/322793.

44. Dubourdeau M, Athman R, Balloy V, Philippe B, Sengmanivong L, Chignard M, et al. Interaction of Aspergillus fumigatus with the alveolar macrophage. Med Mycol. (2006;44:S213–S217. doi:10.1080/13693780600904900.

45. Gresnigt M, Rekiki A, Rasid O, Savers A, Jouvion G, Dannaoui E, et al. Reducing hypoxia and inflammation during invasive pulmonary aspergillosis by targeting the Interleukin-1 receptor. Sci Rep. 2016;6:26490. doi:10.1038/srep26490.

46. Hohl T, Van Epps H, Rivera A, Morgan L, Chen P, *et al* . Aspergillus fumigatus Triggers Inflammatory Responses by Stage-Specific b-Glucan Display. PLOS Pathogens. 2005;1(3):e30. doi:https://doi.org/10.1371/journal.ppat.0010030.

47. Teschner D, Cholaszczynska A, Ries F, Beckert H, Theobald M, Grabbe S, et al. CD11b Regulates Fungal Outgrowth but Not Neutrophil Recruitment in a Mouse Model of Invasive Pulmonary Aspergillosis. Front Immunol. 2019;10:123. doi:10.3389/fimmu.2019.00123.

48. Paisley D, Robson GD, Denning DW. Correlation between in vitro growth rate and in vivo virulence in Aspergillus fumigatus. Medical Mycology. 2005;43(5):397–401. doi:10.1080/13693780400005866.

49. Schrettl M, Bignell E, Kragl C, Joechl C, Rogers T, Arst J Herbert N, et al. Siderophore Biosynthesis But Not Reductive Iron Assimilation Is Essential for Aspergillus fumigatus Virulence. J Exp Med. 2004;200(9):1213–1219. doi:10.1084/jem.20041242.

50. Schrettl M, Bignell E, Kragl C, Sabiha Y, Loss O, Eisendle M, et al. Distinct roles for intra- and extracellular siderophores during Aspergillus fumigatus infection. PLoS Pathog. 2007;3(9):1195–207. doi:10.1371/journal.ppat.0030128.

51. Ewald J, Rivieccio F, Radosa L, Schuster S, Brakhage AA, Kaleta C. Dynamic optimization reveals alveolar epithelial cells as key mediators of host defense in invasive aspergillosis. bioRxiv. 2021;doi:10.1101/2021.05.12.443764.

Multiscale mechanistic modelling of the host defense in invasive aspergillosis reveals leukocyte activation and iron acquisition as drivers of infection outcome
Supplementary Material

Henrique AL Ribeiro, et al.

October 25, 2021

S1 The Parameters

Table S1: Table with the model parameters. Parameters 1-14 were obtained in a unified manner as described in the manuscript. As mentioned in the manuscript, "macrophage" should be interpreted as "macrophage/monocyte." Probabilities of phagocytosis, killing, and interaction refer to the likelihood of an event succeeding in one iteration if the appropriate conditions apply. The maximum number of cells and the average number of epithelial cells is computed over the whole simulated space.

Id	Parameter	Description	Value	Reference
1	MA_IL6_QTTY	Macrophage/monocyte IL6 secretion rate.	$1.46 \times 10^{-20}\ mol * cell^{-1} * h^{-1}$	[1, 2, 3, 4, 5, 6, 7, 8, 9, 10, 11, 12, 13, 14, 15, 16, 17, 18, 19, 20, 21, 22, 23, 24, 25, 26, 27, 28, 29, 30]
2	MA_CCL4_QTTY	Macrophage/monocyte CCL4 secretion rate	$1.79 \times 10^{-20}\ mol * cell^{-1} * h^{-1}$	
3	MA_CXCL2_QTTY	Macrophage/monocyte CXCL2 secretion rate.	$1.11 \times 10^{-19}\ mol * cell^{-1} * h^{-1}$	
4	MA_IL10_QTTY	Macrophage/monocyte IL10 secretion rate.	$6.97 \times 10^{-22}\ mol * cell^{-1} * h^{-1}$	
5	MA_TNF_QTTY	Macrophage/monocyte TNF secretion rate.	$3.22 \times 10^{-20}\ mol * cell^{-1} * h^{-1}$	
6	MA_TGF_QTTY	Macrophage/monocyte $TGF - \beta$ secretion rate.	$1.01 \times 10^{-21}\ mol * cell^{-1} * h^{-1}$	
7	N_IL6_QTTY	Neutrophil IL6 secretion rate.	$8.59 \times 10^{-23}\ mol * cell^{-1} * h^{-1}$	
8	N_CXCL2_QTTY	Neutrophil CXCL2 secretion rate.	$6.50 \times 10^{-22}\ mol * cell^{-1} * h^{-1}$	
9	N_TNF_QTTY	Neutrophil TNF secretion rate.	$1.89 \times 10^{-22}\ mol * cell^{-1} * h^{-1}$	
10	E_IL6_QTTY	Epithelial cell IL6 secretion rate.	$1.46 \times 10^{-20}\ mol * cell^{-1} * h^{-1}$	
11	E_CCL4_QTTY	Epithelial cell CCL4 secretion rate	$1.79 \times 10^{-20}\ mol * cell^{-1} * h^{-1}$	
12	E_CXCL2_QTTY	Epithelial cell CXCL2 secretion rate.	$1.11 \times 10^{-19}\ mol * cell^{-1} * h^{-1}$	
13	E_TNF_QTTY	Epithelial cell TNF secretion rate.	$3.22 \times 10^{-20}\ mol * cell^{-1} * h^{-1}$	
14	LAC_QTTY	Lactoferrin secretion rate (Neutrophils)	$4.37 \times 10^{-17}\ mol * cell^{-1} * h^{-1}$	[31]
15	k_d_IL6	IL-6 k_d	330 pM	[32, 33, 34]
16	k_d_CCL4	CCL4 k_d	180 pM	[35]
17	k_d_CXCL2	CXCL2 k_d	91.667 pM	[36, 37]
18	k_d_IL10	IL-10 k_d	140 pM	[38, 39, 40, 41]
19	k_d_TNF	TNF k_d	326 pM	[42, 43, 44, 45, 46, 47, 48, 49]
20	$k_d_TGF - \beta$	$TGF - \beta$ k_d	26.5 pM	[50, 51, 52]

21	k_d_HEP	Hepcidin k_d	855 nM	[53]
22	D	Diffusion rate	850 $\mu m^2/min$	[54, 55]
23	λ	Cytokine/chemokine half-life	1h	[56, 57, 58, 59, 60, 61, 62]
24	λ_{ab}	Antibody half-life (Anti-TNF)	5 days	[63]
25	HEP_INT	Hepcidin intercept (IL6-hepcidin model)	-0.3141	[64]
26	HEP_SLOPE	Hepcidin slope (IL6-hepcidin model)	0.78	[64]
27	Tf_INT	Transferrin intercept (Tf-hepcidin model)	-1.194×10^{-5}	[65]
28	Tf_SLOPE	Transferrin slope (Tf-hepcidin model)	-5.523×10^{-6}	[65]
29	$Def_TF_CON.$	Default Tf concentration	32.25 μM	[66, 64, 65]
30	$APO_Tf_REL_CON$	Apo-Tf relative concentration	40%	[66, 67]
31	$TfFe_REL_CON$	Monoferric Transferrin relative concentration	16.57%	
32	$TfFe2_REL_CON$	Diferric Transferrin relative concentration	43.43%	
33	MA_IRON_EXP	Macrophage iron export rate	$1367.30 M^{-1} * h^{-1}$	[68]
34	MA_IRON_IMP	Macrophage iron uptake rate	$5.33 \times 10^{-12} L * cell^{-1} * h^{-1}$	[68]
35	MA_INT_IRON	Macrophage initial internal iron quantity	$1.0086 \times 10^{-14} mol$	[66]
36	$TAFC_QTTY$	TAFC secretion rate.	$1.0 \times 10^{-15}\ mol * cell^{-1} * h^{-1}$	[69]
37	$TAFCBI_UPTAKE$	TAFCBI (Bound to Iron) uptake rate	$1 \times 10^{-12} L * cell^{-1} * h^{-1}$	[70, 71]
38	$k_d_Af_IRON$	*A. fumigatus* iron sensitivity	79.05 μM	[72]
39	K_{cat}/K_M_TAFC*	K_{cat}/K_M TAFC-Tf	397.77 $M^{-1}s^{-1}$	[69, 67]
40	K_{cat}/K_M_LAC*	K_{cat}/K_M Lactoferrin-Tf.	399.2 $M^{-1}s^{-1}$	[31]
41	K_{cat}_AB	K_{cat} Antibody-Antigen	120 s^{-1}	[73]
42	K_M_AB	K_M Antibody-Antigen	0.697 μM	[73]
43	AB_CON	Antibody systemic concentration upon injection	0.2 nM	[74]
44	r	*A. fumigatus* growth rate	41.3 $\mu m/h$	[75, 76, 77, 78]
45	MV_RT	Leukocyte movement rate	1.44 $\mu m/min$	[79]
46	N_H_KILL	Neutrophil-hyphae killing probability	22.71%.	[80, 81, 82, 83]
47	MA_H_KILL	Macrophage-hyphae killing probability.	9.85%	[84, 85]
48	MA_PHAG	Macrophage phagocytosis probability	90.55%	[86, 87]
49	N_PHAG	Neutrophil phagocytosis probability	14.73%	[83]
50	$MA_MAX_CONIDIA$	Max ingested conidia by macrophage	18	[87]
51	$N_MAX_CONIDIA$	Max ingested conidia by neutrophils	3	[87, 88]
52	E_INT	Resting epithelial cell-*Aspergillus* interaction probability	4.49%	[89]
53	$PHAG_KILL$	Probability of killing internalized conidia (leukocytes)	1.28%	[90]

54	MA_HALF_LIFE	Macrophage/monocyte half-life	24h	[91]
55	N_HALF_LIFE	Neutrophil half-life	6h	[92]
56	$SEPTAE_r$	Septae radius	2.65 μm	[93, 94, 95]
57	$SEPTAE_L$	Septae length	40 μm	[95, 96]
58	T_SWELL	Time to start swelling	4h	[97]
59	PR_SW	Swelling probability	0.39%	[77, 98]
60	$ITER_GER$	Time until germination (after swelling)	2h	[97]
61	$ITER_CH_ST$	Iterations to cell state change	60	[99]
62	$INTER_REST$	Iterations until active cells return to resting	180	[99]
63	H_VOL	Hyphae volume	1.06 pL	[93, 94, 95, 96]
64	MA_VOL	Macrophage volume	4.85 pL	[100]
65	$CONIDIA_VOL$	Conidia volume	0.0484 pL	[94]
66	PR_BR	Probability of branching (*A. fumigatus*)	25%	[101, 75]
67	$TURNOVER_RT$	Molecule exchange rate between lung and whole body serum.	0.1823 h^{-1}	[102]
68	MAX_N	Maximum number of neutrophils	522	[103]
69	MIN_N	Minimum number of neutrophils	0	[104]
70	MAX_MA	Maximum number of macrophages	209	[103]
71	MIN_MA	Minimum number of macrophages	15	[104]
72	AVG_E	Average number of epithelial cells	640	[105]
73	REC_RT	Global recruitment rate	2	[104]
74	Af_INIT_IRON	*A. fumigatus* initial iron.	$3.83 \times 10^{-18} mol$	[94, 72]

* K_{cat} equal to $1h^{-1}$.

S2 Parameter Acquisition

The model parameters are described in Table S1. In some cases, acquiring these values involved modeling, simplification, and some assumptions. In some cases, we use the MATLAB App Grabit. With this App, one can extract values directly from graphs and pictures. In cases, where more than one measurement is available, the value reported is the median.

S2.1 Cytokine and chemokine secretion rate

The selection of these rates was done using a collection of papers that report the secretion of cytokines in response to $\beta - glucan$, *A. fumigatus*, and, in some cases, LPS as a positive control. Each of these papers reports levels of two or more cytokines after monocyte or macrophage exposure with the respective stimulus. Because only papers that reported at least two cytokines were used, it was possible to construct a relationship of relative secretion rates. For instance, note that across experimental procedures, the level of IL-6 is approximately 45% of the level of TNF, while the level of IL-10 is approximately 4.7% of the level of IL-6, etc. Therefore, this relationship specifies that if we secrete y of TNF, then $0.45 \times y$ IL6 will be secreted.

This procedure was adopted because not all papers, notably those with β-glucan, can be quantified. In other words, a response against β-glucan is qualitatively similar to a response against live *A. fumigatus*. However, it is not known which concentration of β-glucan corresponds to which dose of fungus. With this procedure, however, one can use any piece of data with the implication that one has to fit this relationship to the actual secretion rate. However, having the actual secretion rate for only a few or even one cytokine is enough.

For this purpose, some papers for neutrophils and epithelial cells were used that compare cytokine secretion in these cells with macrophages. Therefore, in the model, these cells are scaled versions of macrophages. Neutrophils secrete 5.9% of what macrophages secret, and epithelial cells secrete the same as macrophages. However, none of these cells secrete IL-10 and TGF-β.

The lactoferrin parameter was acquired independently, and it is a rough approximation based on the amount of the protein a neutrophil carries.

S2.2 TAFC secretion and uptake rates

To calculate the TAFC secretion rate, Equation S2.1 was used to model the experiment of Hissen, AHT *et al.* 2004 [69]. This equation is a surrogate model for our simulator. It models conidia swelling and then secreting TAFC:

$$\frac{d^2[TAFC]}{dt^2} + \gamma * \frac{d[TAFC]}{dt} = \gamma * \sigma * C_0. \tag{S2.1}$$

In Equation S2.1, γ is the swelling rate, C_0 is the concentration of conidia in the experiment, and σ is the TAFC secretion rate, the parameter to be estimated. The value of γ is known from the model (Table S1) and C_0 from the paper itself. The initial condition is such that TAFC(4) = 0. That is, TAFC is zero at four hours, which comes from Table S1, to be interpreted as conidia starting to swell at four hours. Figure S1 shows the fitting of Eq S2.1 to the experimental data of Hissen, AHT *et al.* 2004 [69]. It should be noted that only σ is being fitted, and it should also be noted that the best one can obtain from this experiment is an apparent secretion rate.

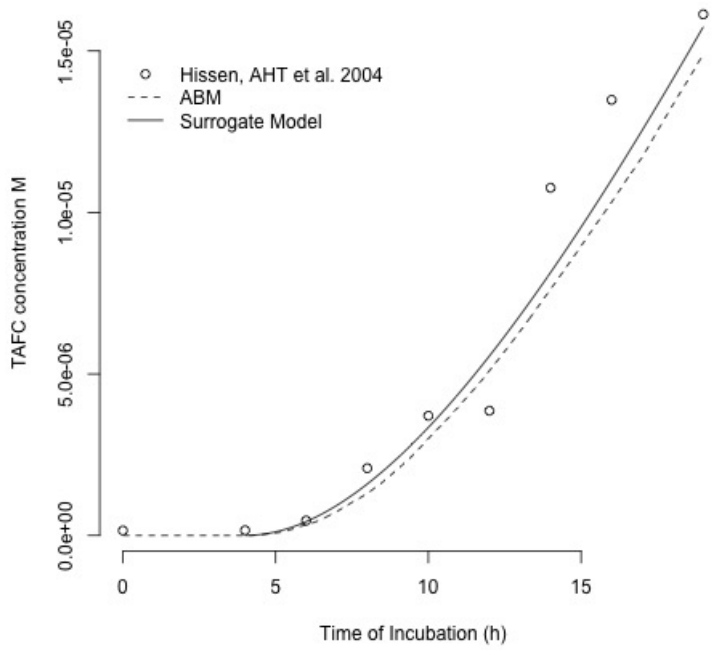

Figure S1: Figure showing the fitting of Eq S2.1. Experimental data from Hissen, AHT *et al.* 2004 [69] (represented as dots in the graph); computed with Eq S2.1 (solid line); computed with the data model (dashed line). Eq S2.1 was computed only from 4h onwards. Before that, we considered no swelling conidia and, therefore, no TAFC production (Table S1). The fact that the full simulator agrees with the surrogate model (Eq S2.1) shows that our procedure was appropriate.

To get the TAFC uptake rate, Raymond-Bouchard, I *et al.* 2012 [70] was used, who reports the TAFC uptake rate as OD600, and Yap, PY *et al.* 2019 [71] reports a curve of OD600 for yeast cells per mL. Supposing that *A. fumigatus* conidia OD600 is similar to that for yeast, one can calculate the TAFC uptake rate per *Aspergillus* cell.

As an approximation, it was assumed that a resting conidium contains one k_d (Section S2.6) of iron, therefore the *Aspergillus* initial amount of iron is $k_d_Af_IRON \times CONIDIA_VOL$ (Table S1).

S2.3 Cytokine and chemokine k_d

The k_d of cytokines/chemokines is divided into two distinct sets of data: the k_d of cytokine/chemokine receptors and dose-response curves for these molecules. As an example of a dose-response curve, consider the level of activation of $NF-\kappa B$ vs. concentration of TNF. It was found that these two approaches are remarkably consistent; that is, activation of a cell by a molecule seems to depend, at least in general, only on the receptor affinity. To model dose-response curves, Equation 2 (Materials & Methods) was used.

S2.4 Iron dynamics

The IL-6-hepcidin and hepcidin-Tf curves were obtained from the literature. While the macrophage iron import rate was also obtained from the literature, the export rate was assumed to be equal to the import rate. Homeostasis is assumed under normal conditions. Equality of iron import and export are interpreted to mean that the fluxes are equal, not the equations' constants. Iron import depends on external iron levels while export depends on internal iron levels.

Values for the internal concentration of macrophage iron, transferrin, and saturation are taken from Parmar, JH *et al.* 2019 [66].

S2.5 Phagocytosis, interaction, and killing rates

A simple law of mass action between leukocytes and conidia is assumed and used to derive Equation, (Eq S2.2). Given time and leukocyte concentration, this equation returns the probability of phagocytosing a conidium. The phagocytosis probability in Table S1 is an extrapolation of Equation S2.2 for a voxel's local concentration and one time step:

$$p = 1 - e^{-k*[L]*t}. \tag{S2.2}$$

In Eq. S2.2, p is the probability of phagocytosis or interaction, [L] is the leukocyte concentration, and t is time, taken to be two minutes in the simulator (one time-step). Note that this extrapolation assumes that the limiting factor in the phagocytosis is the direct interaction between leukocyte and conidia and not the spread rate. According to Hoang, AN *et al.* 2013 [106], the leukocyte movement rate can be quite fast.

The hyphae killing rate is determined similarly. In contrast, the internalized conidia killing rate was acquired based on the percentage of internalized conidia killed by macrophages after 12h. Maximum conidia per macrophage is the apparent maximum reported by Gresnigt, MS *et al.* 2018 [87], and for neutrophils, it is a scaling of this number based on the relative size of a neutrophil.

S2.6 *Aspergillus* iron sensitivity

Aspergillus iron sensitivity ($k_d_Af_IRON$ in Table S1) is a critical parameter in the model. This value measures the concentration of iron needed to turn the sreA gene on/off. This gene, in turn, controls the secretion and uptake of TAFC [107]. As a simplification, this value is also used to control *Aspergillus* growth. Schrettl, M *et al.* 2008 [72] grew WT and sreA KO *Aspergillus* in the presence of TAFCBI (TAFC bound to iron) and then measured the content of iron as μ mol per gram of dry weight (DW) in the colonies.

The first thing to notice is that it is safe to assume that both colonies grew to approximately equal size based on Schrettl, M *et al.* 2008, and others. As mentioned, the paper measures iron in $\mu mol/g$ (DW). To convert this to molar, one can first convert DW into wet weight using data from Bakken, LR, 1983 [93]; this paper also gives the fungal density. With that one is able to calculate molarity.

The sreA KO cannot control the influx of TAFC. Therefore, one can assume, for simplicity, that the iron acquisition in these colonies follows a *quasi-linear* equation (Eq S2.3):

$$\frac{d[Fe_{KO}]}{dt} = k_{up} * h(t) * [TAFC], \tag{S2.3}$$

where k_{up} is the apparent TAFC uptake rate, $h(t)$ is the equation describing hyphal growth, and [TAFC] is the amount of TAFC in the experiment. This is assumed to be constant, that is, the quantity taken up by hyphae is small compared to the amount supplied. Integrating this equation, one gets:

$$[Fe_{KO}] = k_{up} * [TAFC] * \int h(t)dt. \tag{S2.4}$$

This equation gives the quantity of internal iron at the end of the experiment with the sreA KO *Aspergillus*. For WT colonies, as the iron concentration increases, sreA gets activated, which leads to the downregulation of the TAFC receptor. Therefore, for WT, one has:

$$\frac{d[Fe_{WT}]}{dt} = k_{up} * h(t) * [TAFC] * s([Fe_{WT}]). \tag{S2.5}$$

Here, $s([Fe_{WT}])$ is the unknown sreA activation function, but again, one can employ a surrogate model, namely Eq. 2 (Materials & Methods) as a phenomenological model of sreA activation/inactivation. More specifically, this function is used to activate the LIP node that then inactivates the sreA node (see Brandon, M *et al.* 2015 [107]). The function $s([Fe_{WT}])$ should be the complement of that; therefore, Eq S2.5 becomes:

$$\frac{d[Fe_{WT}]}{dt} = k_{up} * h(t) * [TAFC] * e^{-\frac{[Fe_{WT}]}{k_d}}.$$

Integrating this equation one obtains:

$$\int e^{\frac{[Fe_{WT}]}{k_d}} d[Fe_{WT}] = k_{up} * [TAFC] * \int h(t)dt = [Fe_{KO}] + C,$$

where $C = k_d$. Making some algebraic rearrangements results in:

$$[Fe_{WT}] = k_d * \ln(\frac{[Fe_{KO}] + k_d}{k_d}),$$

where $[Fe_{WT}]$ is the quantity of iron in the WT experiment, $[Fe_{KO}]$ is the quantity of iron in the sreA KO experiment, and k_d is the value to be determined. The [TAFC] concentration is assumed to be high, compared to the amount consumed and that $h(t)$ is equal for both sreA KO and WT.

S2.7 Transferrin Michaelis constant

For convenience, Michaelian kinetics is assumed. The TAFC-Tf kinetics is a complex mechanism described by Hissen, AHT & Moore MM 2005 [67] For convenience, a simplified version is used that does not consider cooperativity or difference in transferrin sites. The reaction rate of lactoferrin is very elusive, not having been studied extensively. Nevertheless, one study injected this protein *in vivo* and saw a 46% decrease in serum iron upon 4h [31]. That evidence enables an educated guess of the reaction rate.

S2.8 Fungal biology

Fungal dimensions are obtained from the papers cited in Table S1. In some cases, values can be obtained directly from the photomicrograph reported in these papers using the MATLAB App Grabit. Growth rates come from papers that report hyphal length over time, while branching probability was based on the hyphal growth unit length. This gives an estimate of how many branches per septum there are.

A crucial parameter in the model is the swelling rate. Because swelling is quickly succeeded by germination, the germination rate is used as a proxy for the swelling rate. White, LO 1977 [98] report the rate of germination *in vivo*, and Gago, S *et al.* 2018 [77] report a very consistent value *in vitro* in the presence of bronchoepithelial cells. From these papers, one can make a robust estimate of this value.

S2.9 Number of cells and lung size

Calculations were made by considering a pair of inflated mouse lungs, which has a volume of 1mL [108]. We consider that these pairs of lungs have around 3 million alveoli [109, 110], 230,000 resident macrophages [104], and ten million type-II epithelial cells [105]. The maximum number of mono- and polymorphonuclear cells come from a paper reporting counts of these leukocytes per hundred alveoli in mice infected with *Aspergillus* [103]. The global recruitment rate was adjusted to fit the curve of neutrophils in Bonett, CR *et al.* 2006 [104]. Note that the numbers of macrophages and neutrophils reflect those of bronchoalveolar lavage fluid.

S2.10 Turnover rate

To calculate the turnover rate between the lung and the rest of the body, the following system of differential equations was used:

$$\begin{cases} \frac{dB}{dt} = b(t) - \lambda * B - k * (B - S) \\ \frac{dS}{dt} = k * (B - S) - \lambda * S, \end{cases}$$

where B is the concentration of the molecule in BAL, S is the concentration in serum, and λ is the decay rate. The function $b(t)$ is the secretion rate, and k is the exchange rate, the value to be estimated. The ratio of interest is B/S in the equilibrium. Notice that upon algebraic rearrangements, one finds that this ratio is $(k + \lambda)/k$. But λ is known from the literature (Table S1), and one can estimate k from an empirical B/S ratio found in Gonçalves, SM *et al.* 2017 [102].

S2.11 Leukocyte movement

This movement rate can be obtained from Khandoga, AG *et al.* 2009 [79]. The value, 1.44 $\mu m/min$, is conservative compared to other sources. Pollmacher J, & Figge MT, 2014 [111] uses a movement rate of 2-6 $\mu m/min$, for instance. Nevertheless, the rate used here must be considered a phenomenological movement rate. In the real lung, leukocytes may not move in a straight line but along the alveolar curved surface. That is the case in the Pollmacher J, & Figge MT, 2014 [111] model.

S2.12 Antibodies

Antibody parameters were not specific for TNF. The concentration was obtained based on a measurement of IgG found in mice after an immunization assay. The value of k_{cat} and Km resulted from the imposition of Michaelian kinetics, using data for a generic protein antigen, in this case, the lysosome. Half-life comes from Vieira, P, and Rajewsky K 1988 [63].

S2.13 Other parameters

The time that cells need to change status (T_CHANGE and T_REST) were based on *in-vitro* reports [99]. The half-life of molecules is an average. Likewise, the diffusion rate is an average of the values of the different molecules in living tissue.

For macrophages/monocytes, the 24h value reported for monocytes [91] is used. Other literature sources nevertheless report a longer half-life for macrophages. To calculate macrophage volume, they can be approximated by a sphere, and one can then use the dimensions reported by Krombach, F *et al.* 1997 [100].

S3 Interaction Rules

Table S2: Table with interaction rules. Column one shows the two agents or molecules involved in the interaction. Column three briefly describes the interaction. Column four describes if the interaction is deterministic or probabilistic and if there is an equation involved. Column five describes the outputs of the interaction, that is, how the agent's states are modified upon the interactions and how the concentration of the molecules changes upon the interaction. Notice that an agent can interact with another agent or molecule in more than one way. Therefore, there is some duplication in column two. However, this duplication is eliminated upon the description of the interaction.

Id	Interaction	Description	Type	Outcome	Ref
1	Macrophage-Neutrophil	Macrophage phagocytoses apoptotic neutrophil	Probabilistic: constant probability	Inactivation signal: macrophage changes to inactivating or remains inactive.	[8]
2	Macrophage-Aspergillus	Macrophage phagocytoses swelling conidia	Probabilistic: constant probability	Activating signal: macrophage transitions to activating or remains active; conidia get internalized and subsequently killed	[112, 113, 3]
3	Macrophage-Aspergillus	Active macrophage kills hyphae	Probabilistic: constant probability	Activating signal: macrophage remains active. Hyphae get killed	[3, 84, 85]
4	Macrophage-IL6	Active macrophage secretes IL6	Deterministic: fixed amount	Local IL6 concentration increases	[11, 22, 5, 9, 20, 2, 114]
5	Macrophage-IL10	Active or inactive macrophage secretes IL10	Deterministic: fixed amount	Local IL10 concentration increases	[5, 9, 13, 20, 114]
6	Macrophage-TGF	Inactive macrophage secretes TGF	Deterministic: fixed amount	Local TGF concentration increases	[5, 9, 13, 20, 114]
7	Macrophage-TNF	Active macrophage secretes TNF	Deterministic: fixed amount	Local TNF concentration increases	[5, 9, 13, 20, 2, 4, 115, 114, 1]
8	Macrophage-CCL4	TNF-primed macrophage secretes CCL4[1]	Deterministic: fixed amount	Local CCL4 concentration increases	[114, 1]

9	Macrophage-CXCL2	TNF-primed macrophage secretes CXCL2[1]	Deterministic: fixed amount	Local CXCL2 concentration increases	[4, 115]
10	Macrophage-Hepcidin	Macrophage is primed by Hepcidin	Probabilistic: probability computed according to Equation 6	Macrophage stop exporting iron	[116]
11	Macrophage-IL10	Macrophage is primed by IL10	Probabilistic: probability computed according to Equation 6	Inactivation signal: macrophage transitions to inactivating or remains inactive.	[117]
12	Macrophage-TGF	Macrophage is primed by TGF	Probabilistic: probability computed according to Equation 6	Inactivation signal: macrophage transitions to inactivating or remains inactive.	[8, 7]
13	Macrophage-TNF	Macrophage is primed by TNF	Probabilistic: probability computed according to Equation 6	Activating signal: macrophage transitions to activating; if it is active it moves to TNF-primed and starts secreting chemokines.	[26]
14	Macrophage-Transferrin	Macrophage imports/exports iron from/to transferrin	Deterministic: import/export quantity is proportional to the external and internal levels of transferrin bound to iron (TfFe + TfFe2) and internal levels of iron.	Internal and external levels of iron and transferrin bound to iron(TfFe + TfFe2) change	[68, 118, 119, 120]
15	Neutrophil-IL6	Active neutrophil secretes IL6	Deterministic: fixed amount	Local IL6 concentration increases	[18]
16	Neutrophil-TNF	Active neutrophil secretes TNF	Deterministic: fixed amount	Local TNF concentration increases	[121, 18, 122, 123]
17	Neutrophil-Lactoferrin	Active neutrophil secretes lactoferrin	Deterministic: fixed amount	Local lactoferrin concentration increases	[124, 125]
18	Neutrophil-CCL4	TNF-primed neutrophil secretes CCL4[1]	Deterministic: fixed amount	Local CCL4 concentration increases	[114, 122]
19	Neutrophils-CXCL2	TNF-primed neutrophil secretes CXCL2[1]	Deterministic: fixed amount	Local CXCL2 concentration increases	[122, 123]
20	Neutrophils-TNF	Neutrophil is primed by TNF	Probabilistic: probability computed according to Equation 6	Activating signal: neutrophil transitions to activating; if it is active it moves to TNF-primed and starts secreting chemokines.	[121]
21	Neutrophil-Aspergillus	Neutrophil phagocytoses swelling conidia	Probabilistic: constant probability	Activating signal: neutrophil transitions to activating or remains active; conidia get internalized and subsequently killed	[125]
22	Neutrophil-Aspergillus	Neutrophil kills hyphae	Probabilistic: constant probability	Activating signal: neutrophil transitions to activating or remains active; hyphae are killed	[112, 125]
23	Penumocyte-Aspergillus	Pneumocyte interacts with swelling conidia or hyphae	Probabilistic: initial interaction has a fixed probability, but once interaction is established it is stable.	Activating signal: pneumocyte transitions to activating or remains active;	[126, 127]
24	Pneumocyte-IL6	pneumocyte secretes IL6	Deterministic: fixed amount	Local IL6 concentration increases	[128]
25	Pneumocyte-TNF	Pneumocyte secretes TNF	Deterministic: fixed amount	Local TNF concentration increases	[30]
26	Pneumocyte-CCL4	TNF-primed pneumocyte secretes CCL4	Deterministic: fixed amount	Local CCL4 concentration increases	[129]
27	Pneumocyte-CXCL2	TNF-primed pneumocyte secretes CXCL2	Deterministic: fixed amount	Local CXCL2 concentration increases	[129]
28	Pneumocyte-TNF	Pneumocyte is primed by TNF	Probabilistic: probability computed according to Equation 6	Activating signal: pneumocyte transitions to activating; if it is active it moves to TNF-primed and starts secreting chemokines.	[30]
29	Aspergillus-TAFC	Aspergillus with TAFC node ON secretes TAFC	Deterministic: fixed amount	Local TAFC concentration increases	[107, 130, 72]
30	Aspergillus-TAFC	Aspergillus with nodes MirB and EstB ON uptake TAFC-Bound to Iron	Deterministic: proportional to the concentration of TAFC- Bound to Iron	Local concentration of TAFC Bound to Iron decreases; Aspergillus Iron Pool increases, increasing the probability of activating LIP node	[107, 70]

31	TAFC-Transferrin	TAFC sequesters iron from transferrin bound to iron (TfFe +TfFe2)	Deterministic: reaction proceeds according to Equation 7	Local levels of TAFC-free and Transferrin Bound to Iron decrease while levels of TAFC Bound to Iron and free transferrin increase.	[130, 69]
32	Lactoferrin-Transferrin	Lactoferrin sequesters iron from Transferrin Bound to Iron (TfFe + TfFe2)	Deterministic: reaction proceeds according to Equation 7	Local levels of free lactoferrin and Transferrin Bound to Iron decrease while levels of Lactoferrin Bound to Iron (LTfFe + LTfFe2) and free transferrin increase.	[31, 131]
33	Macrophage-iron	Necrotic macrophage releases its iron content[2]	Deterministic: whole iron content of the cell is released	Local iron concentration increases	
34	Aspergillus-Iron	Dead-Aspergillus releases its iron content[2]	Deterministic: whole cell iron content is released	Local iron concentration increases	
35	TAFC-Iron	TAFC sequesters Fe^3	Deterministic: TAFC sequesters the whole iron content in the voxel or the maximum of its capacity	free TAFC and iron decrease; TAFC bound to iron increases	
36	Transferrin-Iron	Transferrin sequesters Fe^3	Deterministic: transferrin sequesters the whole iron content in the voxel or the maximum of its capacity	free transferrin and iron decrease; Transferrin Bound to Iron increases	
37	Lactoferrin-Iron	Lactoferrin sequesters Fe^3	Deterministic: lactoferrin sequesters the whole iron content in the voxel or the maximum of its capacity	free lactoferrin and iron decrease; Transferrin Bound to Iron increases	

We are using here the macrophage nomenclature used by Gordon, S 2003 [132] where $TGF - \beta$ secreting macrophages are called inactive. This is equivalent to the M2c macrophages referred by Duque, GA & Descoteaux, A 2014 [133].

S4 Drivers of Fungal Burden

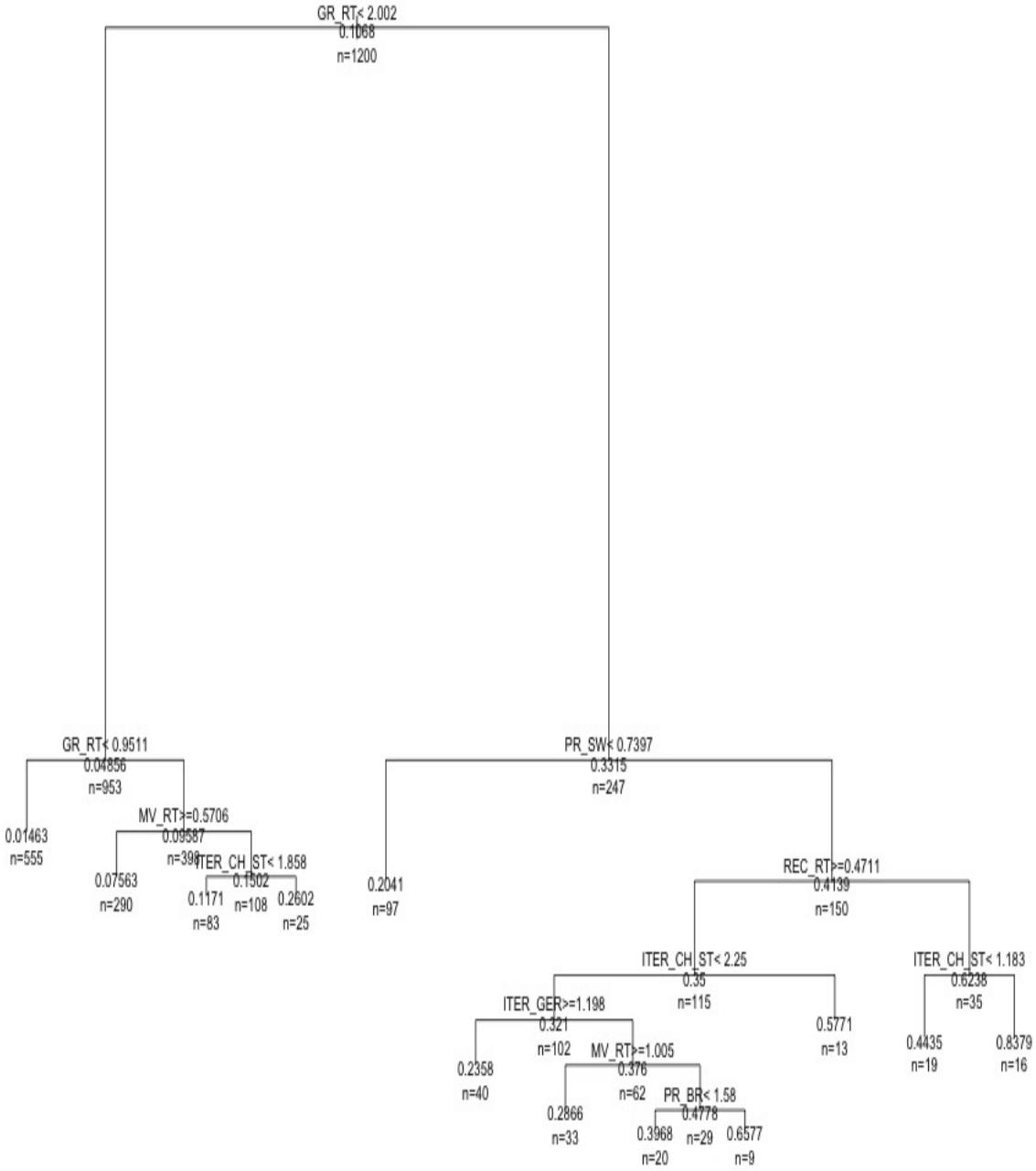

Figure S2: Classification trees of fungal burden. We generated 1200 samples with LHS and ran simulations with immunocompetent hosts, and classified the simulations by the maximum number of hyphal cells measured over 24 hours of simulation. For convenience, all the parameters were normalized by their default values. That is, a value of 2 means that the tree made a partition when that parameter was twice its default value (Table S1). We also normalized the fungal burden by the initial dose inocula (1920 conidia). Notice, however, that the measure of fungal burden is the maximum number of hyphal cells encountered at any time over a 24 hour period. This counts only the conidia that germinate and the hyphae that multiply, excluding ungerminated conidia.

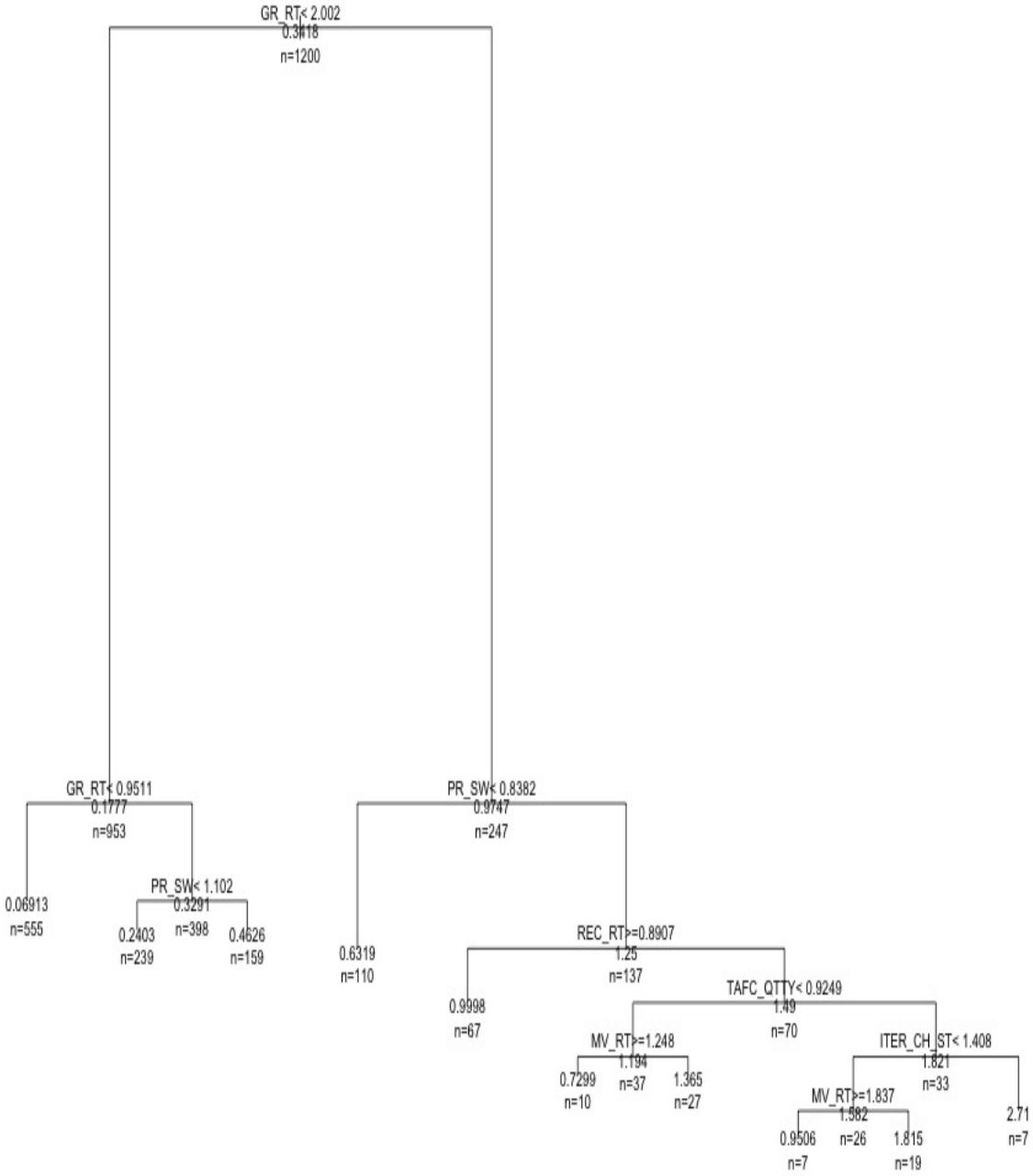

Figure S3: Classification trees of fungal burden. We generated 1200 samples with LHS and ran simulations with neutropenic hosts, and classified the simulations by the maximum number of hyphal cells measured over 24 hours of simulation. For convenience, all the parameters were normalized by their default values. That is, a value of 2 means that the tree made a partition when that parameter was twice its default value (Table S1). We also normalized the fungal burden by the initial dose inocula (1920 conidia). Notice, however, that the measure of fungal burden is the maximum number of hyphal cells encountered at any time over a 24 hour period. This counts only the conidia that germinate and the hyphae that multiply, excluding ungerminated conidia.

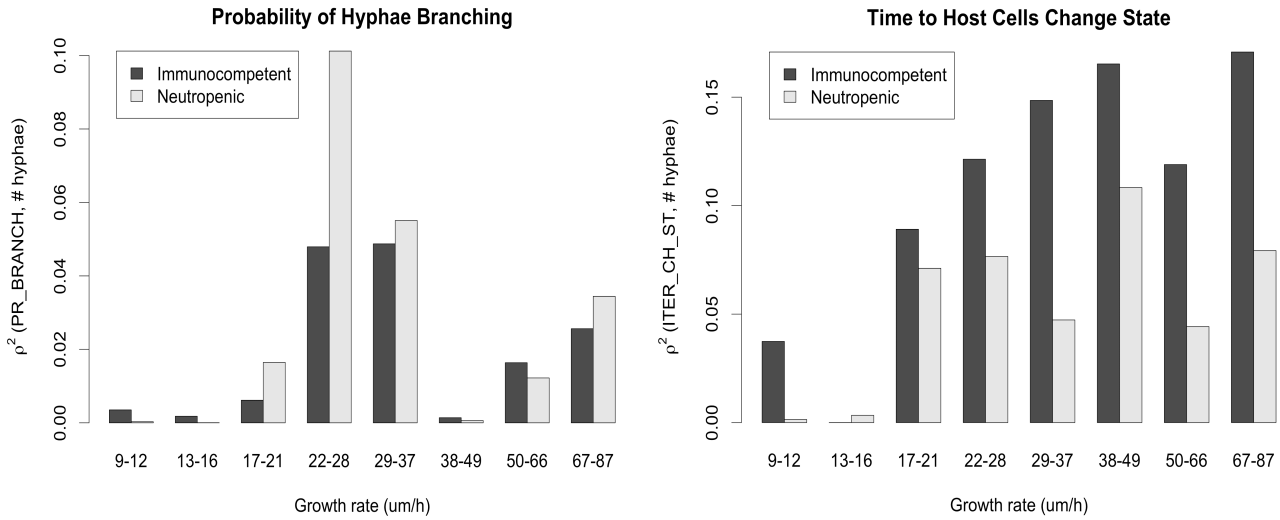

A B

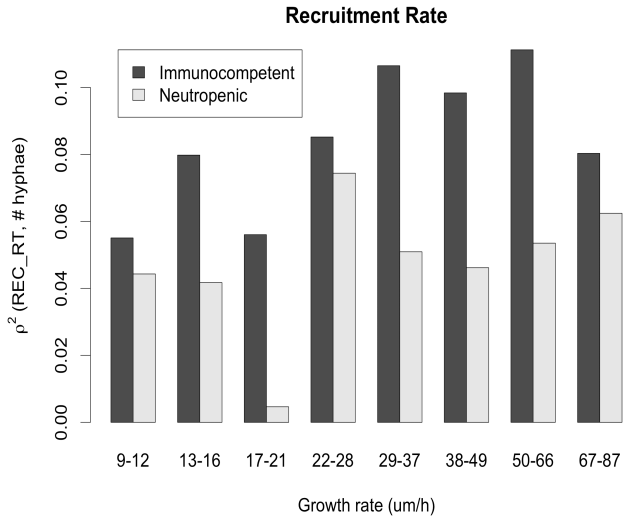

C

Figure S4: Variation of the square of the correlation r^2 between the critical model parameters and fungal burden, as the growth rate varies along the x-axis. We started with a dataset of 1200 samples generated with LHS and then partitioned this dataset by growth rate. The x-axis in the figure shows the range of the growth rate in each partition. We then calculate the correlation between parameters and fungal burden in each partition. Fungal burden was the maximum number of hyphal cells measured over the course of 24 hours of simulation. A: variation of r^2 between the probability of branching and fungal burden. B: variation of r^2 between the iterations for host cells to change state and fungal burden. C: variation of r^2 between the leukocyte recruitment rate and fungal burden.

References

[1] Werner JL, Metz AE, Horn D, Schoeb TR, Hewitt MM, Schwiebert LM, et al. Requisite Role for the Dectin-1 b-Glucan Receptor in Pulmonary Defense against Aspergillus fumigatus. The Journal of Immunology. 2009;182(8):4938–4946. doi:10.4049/jimmunol.0804250.

[2] Taylor P, Tsoni S, Willment J, *et al* . Dectin-1 is required for β-glucan recognition and control of fungal infection. Nat Immunol. 2007;8:31–38. doi:https://doi.org/10.1038/ni1408.

[3] Gersuk GM, Underhill DM, Zhu L, Marr KA. Dectin-1 and TLRs Permit Macrophages to Distinguish between Different Aspergillus fumigatus Cellular States. The Journal of Immunology. 2006;176(6):3717–3724. doi:10.4049/jimmunol.176.6.3717.

[4] Hohl T, Van Epps H, Rivera A, Morgan L, Chen P, *et al* . Aspergillus fumigatus Triggers Inflammatory Responses by Stage-Specific b-Glucan Display. PLOS Pathogens. 2005;1(3):e30. doi:https://doi.org/10.1371/journal.ppat.0010030.

[5] Chai L, Netea M, Sugui J, Vonk A, van de Sande W, Warris A, et al. Aspergillus fumigatus conidial melanin modulates host cytokine response. Immunobiology. 2010;215(11):915–920. doi:10.1016/j.imbio.2009.10.002.

[6] Mark BH, Anthony JK, Christine CW. Inside the Neutrophil Phagosome: Oxidants, Myeloperoxidase, and Bacterial Killing. Blood. 1998;92(9):3007–3017. doi:https://doi.org/10.1182/blood.V92.9.3007.

[7] Celio GFdL, Xiao YQ, Shyra JG, Donna LB, William PS, Peter MH. Apoptotic Cells, through Transforming Growth Factor-β, Coordinately Induce Anti-inflammatory and Suppress Pro-inflammatory Eicosanoid and NO Synthesis in Murine Macrophages. J Biol Chem. 2006;281:38376–. doi:10.1074/jbc.M605146200.

[8] Fadok VA, Bratton DL, Konowal A, Freed PW, Westcott JY, Henson PM. Macrophages that have ingested apoptotic cells in vitro inhibit proinflammatory cytokine production through autocrine/paracrine mechanisms involving TGF-beta, PGE2, and PAF. The Journal of Clinical Investigation. 1998;101(2). doi:10.1172/JCI1112.

[9] Steele C, Rapaka R, Metz A, Pop S, Williams D, *et al* . The Beta-Glucan Receptor Dectin-1 Recognizes Specific Morphologies of Aspergillus fumigatus. PLOS Pathogens. 2005;1(4):e42. doi:doi.org/10.1371/journal.ppat.0010042.

[10] Adachi Y, Okazaki M, Ohno N, Yadomae T. Enhancement of cytokine production by macrophages stimulated with (1–¿3)-beta-D-glucan, grifolan (GRN), isolated from Grifola frondosa. Biol Pharm Bull. 1994;17(12):1554–1560. doi:10.1248/bpb.17.1554.

[11] Okazaki M, Adachi Y, Ohno N, Yadomae T. Structure-activity relationship of (1–¿3)-beta-D-glucans in the induction of cytokine production from macrophages, in vitro. Biol Pharm Bull 1995 Oct;18. 10;18(10):1320–7. doi:10.1248/bpb.18.1320.

[12] Brummer E, Kamberi M, Stevens DA. Regulation by Granulocyte-Macrophage Colony-Stimulating Factor and/or Steroids Given In Vivo of Proinflammatory Cytokine and Chemokine Production by Bronchoalveolar Macrophages in Response to Aspergillus Conidia. The Journal of Infectious Diseases,. 2003;187(4):705–709. doi:doi.org/10.1086/368383.

[13] Mihai GN, Warris A, Jos WMVdM, Matthew JF, Trees JGVJ, Liesbeth EHJ, et al. Aspergillus fumigatus Evades Immune Recognition during Germination through Loss of Toll-Like Receptor-4-Mediated Signal Transduction. The Journal of Infectious Diseases,. 2003;188(2):320–326. doi:doi.org/10.1086/376456.

[14] Marika K, Elmer B, Davidm AS. Regulation of Bronchoalveolar Macrophage Proinflammatory Cytokine Production By Dexamethasone and Granulocyte-Macrophage Colony-Stimulating Factor After Stimulation By Aspergillus Conidia Or Lipopolysaccharide. Cytokine,. 2002;19(1):14–20. doi:doi.org/10.1006/cyto.2002.1049.

[15] Warris A, Netea M, Verweij P, Gaustad P, Kullberg B, Weemaes C, et al. Cytokine responses and regulation of interferon-gamma release by human mononuclear cells to Aspergillus fumigatus and other filamentous fungi. Med Mycol. 2005;43(7):613–21. doi:10.1080/13693780500088333.

[16] Fadok VA, Bratton DL, Guthrie L, Henson PM. Differential Effects of Apoptotic Versus Lysed Cells on Macrophage Production of Cytokines: Role of Proteases. J Immunol. 2001;166(11):6847–6854. doi:10.4049/jimmunol.166.11.6847.

[17] Fujishima S, Hoffman AR, Vu KJ T Kim, Zheng H, Daniel D, Kim W Y, et al. Regulation of neutrophil interleukin 8 gene expression and protein secretion by LPS, TNF-α, and IL-1β. J Cell Physiol,. 1993;154:478–485. doi:10.1002/jcp.1041540305.

[18] Xing L, Remick D. Relative cytokine and cytokine inhibitor production by mononuclear cells and neutrophils. Shock. 2003;20(1):10–6. doi:10.1097/01.shk.0000065704.84144.a4.

[19] Altstaedt J, Kirchner H, Rink L. Cytokine production of neutrophils is limited to interleukin-8. Immunology,. 1996;89:563–568. doi:10.1046/j.1365-2567.1996.d01-784.x.

[20] Bondeson J, Browne K, Brennan F, Foxwell B, Feldmann M. Selective regulation of cytokine induction by adenoviral gene transfer of IkappaBalpha into human macrophages: lipopolysaccharide-induced, but not zymosan-induced, proinflammatory cytokines are inhibited, but IL-10 is nuclear factor-kappaB independent. J Immunol. 1999;162(5):2939–45.

[21] Abe Y, Hashimoto S, Horie T. Curcumin inhibition of inflammatory cytokine production by human peripheral blood monocytes and alveolar macrophages. Pharmacol Res. 1999;39(1):41–7. doi:10.1006/phrs.1998.0404.

[22] Loeffler J, Haddad Z, Bonin M, Romeike N, Mezger M, Schumacher U, et al. Interaction analyses of human monocytes co-cultured with different forms of Aspergillus fumigatus. Journal of Medical Microbiology. 2009;58(1):49–58. doi:doi.org/10.1099/jmm.0.003293-0.

[23] Simitsopoulou M, Roilides E, Likartsis C, Ioannidis J, Orfanou A, Paliogianni F, et al. Expression of Immunomodulatory Genes in Human Monocytes Induced by Voriconazole in the Presence of Aspergillus fumigatus. Antimicrobial Agents and Chemotherapy. 2007;51(3):1048–1054. doi:10.1128/AAC.01095-06.

[24] Lord PC, Wilmoth LM, Mizel SB, McCall CE. Expression of interleukin-1 alpha and beta genes by human blood polymorphonuclear leukocytes. The Journal of Clinical Investigation. 1991;87(4):1312–1321. doi:10.1172/JCI115134.

[25] Cassatella M. The production of cytokines by polymorphonuclear neutrophils. Immunol Today. 1995;16(1):21–6. doi:10.1016/0167-5699(95)80066-2.

[26] Ciesielski C, Andreakos E, Foxwell B, Feldmann M. TNFa-induced macrophage chemokine secretion is more dependent on NF-kB expression than lipopolysaccharides-induced macrophage chemokine secretion. European Journal of Immunology. 2002;32(7):2037–2045. doi:https://doi.org/10.1002/1521-4141(200207)32:7¡2037::AID-IMMU2037¿3.0.CO;2-I.

[27] Palmberg L, Larsson B, Malmberg P, Larsson K. Induction of IL-8 production in human alveolar macrophages and human bronchial epithelial cells in vitro by swine dust. Thorax. 1998;53(4):260–4. doi:10.1136/thx.53.4.260.

[28] Jablonski H, Rekasi H, Jager M. The influence of calcitonin gene-related peptide on markers of bone metabolism in MG-63 osteoblast-like cells co-cultured with THP-1 macrophage-like cells under virtually osteolytic conditions. BMC Musculoskelet Disord. 2016;17(199.). doi:doi.org/10.1186/s12891-016-1044-5.

[29] Katsuo K, Bo-Ram O. Optofluidic cellular immunofunctional analysis by localized surface plasmon resonance. Proc SPIE 9166, Biosensing and Nanomedicine VII, 91660R. 2014;doi:doi.org/10.1117/12.2062244.

[30] Thorley AJ, Ford PA, Giembycz MA, Goldstraw P, Young A, Tetley TD. Differential Regulation of Cytokine Release and Leukocyte Migration by Lipopolysaccharide-Stimulated Primary Human Lung Alveolar Type II Epithelial Cells and Macrophages. The Journal of Immunology. 2007;178(1):463–473. doi:10.4049/jimmunol.178.1.463.

[31] Jacques LvS, Pierre LM, Joseph FH. The Involvement Of Lactoferrin In The Hyposideremia Of Acute Inflammation. J Exp Med. 1974;140(4):1068–1084. doi. doi:https://doi.org/10.1084/jem.140.4.1068.

[32] Taga T, Hibi M, Hirata Y, Yamasaki K, Yasukawa K, Matsuda T, et al. Interleukin-6 triggers the association of its receptor with a possible signal transducer, gp130. Cell. 1989;58(3):573–81. doi:10.1016/0092-8674(89)90438-8.

[33] Gaillard J, Pugnière M, Tresca J, Mani J, Klein B, Brochier J. Interleukin-6 receptor signaling. II. Bio-availability of interleukin-6 in serum. Eur Cytokine Netw. 1999;10(3):337–44.

[34] Zohlnhöfer D, Graeve L, Rose-John S, Schooltink H, Dittrich E, Heinrich P. The hepatic interleukin-6 receptor. Down-regulation of the interleukin-6 binding subunit (gp80) by its ligand. FEBS Lett. 1992;306(2-3):219–22. doi:10.1016/0014-5793(92)81004-6.

[35] Samson M, LaRosa G, Libert F, Paindavoine P, Detheux M, Vassart G, et al. The second extracellular loop of CCR5 is the major determinant of ligand specificity. J Biol Chem. 1997;272(40):24934–24941. doi:10.1074/jbc.272.40.24934.

[36] Sai J, Fan GH, Wang D, Richmond A. The C-terminal domain LLKIL motif of CXCR2 is required for ligand-mediated polarization of early signals during chemotaxis. Journal of Cell Science. 2004;117(23):5489–5496. doi:10.1242/jcs.01398.

[37] Al-Alwan LA, Chang Y, Mogas A, Halayko AJ, Baglole CJ, Martin JG, et al. Differential Roles of CXCL2 and CXCL3 and Their Receptors in Regulating Normal and Asthmatic Airway Smooth Muscle Cell Migration. The Journal of Immunology. 2013;191(5):2731–2741. doi:10.4049/jimmunol.1203421.

[38] Liu Y, Wei S, Ho A, de Waal MR, Moore K. Expression cloning and characterization of a human IL-10 receptor. J Immunol. 1994;152(4):1821–9.

[39] Tan J, Indelicato S, Narula S, Zavodny P, Chou C. Characterization of interleukin-10 receptors on human and mouse cells. J Biol Chem. 1993;268(28):21053–21059.

[40] Ho AS, Liu Y, Khan TA, Hsu DH, Bazan JF, Moore KW. A receptor for interleukin 10 is related to interferon receptors. Proceedings of the National Academy of Sciences. 1993;90(23):11267–11271. doi:10.1073/pnas.90.23.11267.

[41] Carson W, Lindemann M, Baiocchi R, Linett M, Tan J, Chou C, et al. The functional characterization of interleukin-10 receptor expression on human natural killer cells. Blood. 1995;85(12):3577–85.

[42] Schall T, Lewis M, Koller K, Lee A, Rice G, Wong G, et al. Molecular cloning and expression of a receptor for human tumor necrosis factor. Cell. 1990;61(2):361–70. doi:10.1016/0092-8674(90)90816-w.

[43] Aggarwal B, Eessalu T, Hass P. Characterization of receptors for human tumour necrosis factor and their regulation by γ-interferon. Nature. 1985;318:665–667. doi:doi.org/10.1038/318665a0.

[44] Tsujimoto M, Yip YK, Vilcek J. Tumor necrosis factor: specific binding and internalization in sensitive and resistant cells. Proceedings of the National Academy of Sciences. 1985;82(22):7626–7630. doi:10.1073/pnas.82.22.7626.

[45] Baglioni C, McCandless S, Tavernier J, Fiers W. Binding of human tumor necrosis factor to high affinity receptors on HeLa and lymphoblastoid cells sensitive to growth inhibition. J Biol Chem. 1985;260(25):13395–7.

[46] Tsujimoto M, vilcek J. Tumor Necrosis Factor-Induced Downregulation of Its Receptors in HeLa Cells. The Journal of Biochemistry,. 1987;102(6):1571–1577. doi:doi.org/10.1093/oxfordjournals.jbchem.a122206.

[47] Stauber G, Aiyer R, Aggarwal B. Human tumor necrosis factor-alpha receptor. Purification by immunoaffinity chromatography and initial characterization. J Biol Chem. 1988;263(35):19098–104.

[48] Hohmann H, Remy R, Brockhaus M, van Loon A. Two different cell types have different major receptors for human tumor necrosis factor (TNF alpha). J Biol Chem. 1989;264(25):14927–34.

[49] Ding A, Sanchez E, Srimal S, Nathan C. Macrophages rapidly internalize their tumor necrosis factor receptors in response to bacterial lipopolysaccharide. J Biol Chem. 1989;264(7):3924–9.

[50] Massague J, Like B. Cellular receptors for type beta transforming growth factor. Ligand binding and affinity labeling in human and rodent cell lines. J Biol Chem. 1985;260(5):2636–45.

[51] Kalter VG, Brody AR. Receptors for Transforming Growth Factor-β (TGF-β) on Rat Lung Fibroblasts Have Higher Affinity for TGF-β1 than for TGF-β2. American Journal of Respiratory Cell and Molecular Biology. 1991;4(5):397–407. doi:10.1165/ajrcmb/4.5.397.

[52] Wakefield L, Smith D, Masui T, Harris C, Sporn M. Distribution and modulation of the cellular receptor for transforming growth factor-beta. J Cell Biol. 1987;105(2):965–75. doi:10.1083/jcb.105.2.965. PMID: 2887577.

[53] Nemeth E, Tuttle MS, Powelson J, Vaughn MB, Donovan A, Ward DM, et al. Hepcidin Regulates Cellular Iron Efflux by Binding to Ferroportin and Inducing Its Internalization. Science. 2004;306(5704):2090–2093. doi:10.1126/science.1104742.

[54] Goodhill GJ. Diffusion in Axon Guidance. European Journal of Neuroscience. 1997;9:1414–1421. doi:10.1111/j.1460-9568.1997.tb01496.x.

[55] Goodhill G. Mathematical guidance for axons. Trends in Neurosciences. 1998;21(6):226–231. doi:10.1016/s0166-2236(97)01203-4.

[56] Huhn RD, Radwanski E, Gallo J, Affrime MB, Sabo R, Gonyo G, et al. Pharmacodynamics of subcutaneous recombinant human interleukin-10 in healthy volunteers. Clinical Pharmacology & Therapeutics. 1997;62(2):171–180. doi:https://doi.org/10.1016/S0009-9236(97)90065-5.

[57] Zahn G, Greischel A. Pharmacokinetics of tumor necrosis factor alpha after intravenous administration in rats. Dose dependence and influence of tumor necrosis factor beta. Arzneimittelforschung. 1989;39(9):1180–1182.

[58] Oliver J, Bland L, Oettinger C, Arduino M, McAllister S, Aguero S, et al. Cytokine kinetics in an in vitro whole blood model following an endotoxin challenge. Lymphokine Cytokine Res. 1993;12(2):115–120.

[59] Kuribayashi T. Elimination half-lives of interleukin-6 and cytokine-induced neutrophil chemoattractant-1 synthesized in response to inflammatory stimulation in rats. Lab Anim Res. 2018;34:80–83. doi:https://doi.org/10.5625/lar.2018.34.2.80.

[60] Castell JV, Geiger T, Gross V, Andus T, Walter E, Hirano T, et al. Plasma clearance, organ distribution and target cells of interleukin-6/hepatocyte-stimulating factor in the rat. European Journal of Biochemistry. 1988;177(2):357–361. doi:https://doi.org/10.1111/j.1432-1033.1988.tb14383.x.

[61] Toft A, Falahati A, Steensberg A. Source and kinetics of interleukin-6 in humans during exercise demonstrated by a minimally invasive model. Eur J Appl Physiol. 2011;111:1351–1359. doi:https://doi.org/10.1007/s00421-010-1755-5.

[62] Wakefield L, Winokur T, Hollands R, Christopherson K, Levinson A, Sporn M. Recombinant latent transforming growth factor beta 1 has a longer plasma half-life in rats than active transforming growth factor beta 1, and a different tissue distribution. The Journal of Clinical Investigation. 1990;86(6):1976–1984. doi:10.1172/JCI114932.

[63] Vieira P, Rajewsky K. The half-lives of serum immunoglobulins in adult mice. European Journal of Immunology. 1988;18(2):313–316. doi:https://doi.org/10.1002/eji.1830180221.

[64] Tabbah S, Buhimschi C, Rodewald-Millen K, Pierson C, Bhandari V, Samuels P, et al. Hepcidin, an Iron Regulatory Hormone of Innate Immunity, is Differentially Expressed in Premature Fetuses with Early-Onset Neonatal Sepsis. Am J Perinatol. 2018;35(9):865–872. doi:10.1055/s-0038-1626711.

[65] Moran-Lev H, Weisman Y, Cohen S, Deutsch V, Cipok M, Bondar E, et al. The interrelationship between hepcidin, vitamin D, and anemia in children with acute infectious disease. Pediatr Res. 2018;84(1):62–65. doi:10.1038/s41390-018-0005-0.

[66] Parmar JH, Mendes P. A computational model to understand mouse iron physiology and disease. PLOS Computational Biology. 2019;15(1):1–28. doi:10.1371/journal.pcbi.1006680.

[67] Hissen AHT, Moore MM. Site-specific rate constants for iron acquisition from transferrin by the Aspergillus fumigatus siderophores N',N",N"'-triacetylfusarinine C and ferricrocin. J Biol Inorg Chem 10, 211–220. 2005;10:211–220. doi:https://doi.org/10.1007/s00775-005-0630-z.

[68] Sarkar J, Seshadri V, Tripoulas N, Ketterer M, Fox P. Role of ceruloplasmin in macrophage iron efflux during hypoxia. J Biol Chem. 2003;278(45):44018–24. doi:10.1074/jbc.M304926200.

[69] Hissen AHT, Chow JMT, Pinto LJ, Moore MM. Survival of Aspergillus fumigatus in Serum Involves Removal of Iron from Transferrin: the Role of Siderophores. INFECTION AND IMMUNITY. 2004;72(3):1402–1408.

[70] Raymond-Bouchard I, Carroll CS, Nesbitt JR, Henry KA, Pinto LJ, Moinzadeh M, et al. Structural Requirements for the Activity of the MirB Ferrisiderophore Transporter of Aspergillus fumigatus. Eukaryotic Cell. 2012;11(11). doi:10.1128/EC.00159-12.

[71] Yap PY, Trau D. Direct Yeast Cell Count At OD600. Tip Biosystems Pte Ltd. 2019;2019.

[72] Schrettl M, Kim HS, Eisendle M, Kragl C, Nierman WC, Heinekamp T, et al. SreA-mediated iron regulation in Aspergillus fumigatus. Molecular Microbiology,. 2008;70:27–43. doi:10.1111/j.1365-2958.2008.06376.x.

[73] Goldbaum FA, Cauerhff A, Velikovsky CA, Llera AS, Riottot MM, Poljak RJ. Lack of Significant Differences in Association Rates and Affinities of Antibodies from Short-Term and Long-Term Responses to Hen Egg Lysozyme. The Journal of Immunology. 1999;162(10):6040–6045.

[74] Colino J, Diez M, Outschoorn I. A quantitative ELISA for antigen-specific IgG subclasses using equivalence dilutions of anti-kappa and anti-subclass specific secondary reagents. Application to the study of the murine immune response against the capsular polysaccharide of Neisseria meningitidis serogroup B. J Immunol Methods. 1996;190(2):221–34. doi:10.1016/0022-1759(95)00278-2.

[75] Bocking SP, Wiebe MG, Robson GD, Hansen K, Christiansen LH, Trinci APJ. Effect of branch frequency in Aspergillus oryzae on protein secretion and culture viscosity. Biotechnol Bioeng,. 1999;65:638–648. doi:10.1002/(SICI)1097-0290(19991220)65:6¡638::AID-BIT4¿3.0.CO;2-K.

[76] Escobar N, Ordonez S, Wösten H, Haas P, de Cock H, Haagsman H. Hide, Keep Quiet, and Keep Low: Properties That Make Aspergillus fumigatus a Successful Lung Pathogen. Front Microbiol. 2016;7:438. doi:10.3389/fmicb.2016.00438.

[77] Gago S, Overton NLD, Ben-Ghazzi Nt. Lung colonization by Aspergillus fumigatus is controlled by ZNF77. Nat Commun 9,. 2018;3835. doi:https://doi.org/10.1038/s41467-018-06148-7.

[78] Meletiadis J, Meis JFGM, Mouton JW, Verweij PE. Analysis of Growth Characteristics of Filamentous Fungi in Different Nutrient Media. Journal of Clinical Microbiology. 2001;39(2):478–484. doi:10.1128/JCM.39.2.478-484.2001.

[79] Khandoga A, Khandoga A, Reichel C, Bihari P, Rehberg M, *et al* . In Vivo Imaging and Quantitative Analysis of Leukocyte Directional Migration and Polarization in Inflamed Tissue. PLoS ONE. 2009;4(3):e4693. doi:10.1371/journal.pone.0004693.

[80] Zarember K, Sugui J, Chang Y, Kwon-Chung K, Gallin J. Human polymorphonuclear leukocytes inhibit Aspergillus fumigatus conidial growth by lactoferrin-mediated iron depletion. J Immunol. 2007;178(10):6367–6373. doi:10.4049/jimmunol.178.10.6367.

[81] Gazendam RP, van Hamme JL, Tool AT, Hoogenboezem M, van den Berg JM, Prins JM, et al. Human Neutrophils Use Different Mechanisms To Kill Aspergillus fumigatus Conidia and Hyphae: Evidence from Phagocyte Defects. The Journal of Immunology. 2016;196(3):1272–1283. doi:10.4049/jimmunol.1501811.

[82] Gazendam R, van de Geer A, van Hamme J, Tool A, van Rees D, Aarts C, et al. Impaired killing of Candida albicans by granulocytes mobilized for transfusion purposes: a role for granule components. Haematologica. 2016;101(5):587–96. doi:10.3324/haematol.2015.136630.

[83] Roilides E, Dimitriadou-Georgiadou A, Sein T, Kadiltsoglou I, Walsh T. Tumor necrosis factor alpha enhances antifungal activities of polymorphonuclear and mononuclear phagocytes against Aspergillus fumigatus. Infect Immun. 1998;66(12):5999–6003. doi:10.1128/IAI.66.12.5999-6003.1998.

[84] Roilides E, Sein T, Holmes A, Chanock S, Blake C, Pizzo P, et al. Effects of macrophage colony-stimulating factor on antifungal activity of mononuclear phagocytes against Aspergillus fumigatus. J Infect Dis. 1995;172(4):1028–1034. doi:10.1093/infdis/172.4.1028. PMID: 7561176.

[85] Roilides E, Holmes A, Blake C, Venzon D, Pizzo P, Walsh T. Antifungal activity of elutriated human monocytes against Aspergillus fumigatus hyphae: enhancement by granulocyte-macrophage colony-stimulating factor and interferon-gamma. J Infect Dis. 1994;170(4):894–9. doi:10.1093/infdis/170.4.894.

[86] Philippe B, Ibrahim-Granet O, Prévost M, Gougerot-Pocidalo M, Sanchez PM, Van der Meeren A, et al. Killing of Aspergillus fumigatus by alveolar macrophages is mediated by reactive oxidant intermediates. Infect Immun. 2003;71(6):3034–42. doi:10.1128/iai.71.6.3034-3042.2003.

[87] Gresnigt MS, Becke rKL, Leenders F, Alonso MF, Wang X, Meis JF, et al. Differential Kinetics of Aspergillus nidulans and Aspergillus fumigatus Phagocytosis. J Innate Immun. 2018;10:145–160. doi:10.1159/000484562.

[88] Niemiec M, De Samber B, Garrevoet J, Vergucht E, Vekemans B, De Rycke R, et al. Trace element landscape of resting and activated human neutrophils on the sub-micrometer level. Metallomics. 2015;7(6):996–1010. doi:10.1039/c4mt00346b.

[89] Clark HR, Powell AB, Simmons KA, Ayubi T, Kale SD. Endocytic Markers Associated with the Internalization and Processing of Aspergillus fumigatus Conidia by BEAS-2B Cells. mSphere. 2019;4(1):e00663–18. doi:10.1128/mSphere.00663-18.

[90] Wasylnka J, Hissen A, Wan A, Moore M. Intracellular and extracellular growth of Aspergillus fumigatus. Med Mycol. 2005;43:S27–S30. doi:10.1080/13693780400029247.

[91] Patel A, Zhang Y, Fullerton J, Boelen L, Rongvaux A, Maini A, et al. The fate and lifespan of human monocyte subsets in steady state and systemic inflammation. The Journal of experimental medicine. 2017;214. doi:10.1084/jem.20170355.

[92] Tak T, Tesselaar K, Pillay J, Borghans J, Koenderman L. What's your age again? Determination of human neutrophil half-lives revisited. J Leukoc Biol. 2013;94(4):595–601. doi:10.1189/jlb.1112571.

[93] Bakken L, Olsen R. Buoyant densities and dry-matter contents of microorganisms: conversion of a measured biovolume into biomass. Appl Environ Microbiol. 1983;45(4):1188–1195. doi:10.1128/AEM.45.4.1188-1195.1983.

[94] Sugui J, Kwon-Chung K, Juvvadi P, Latgé J, Steinbach W. Aspergillus fumigatus and related species. Cold Spring Harb Perspect Med. 2014;5(2):a019786. doi:10.1101/cshperspect.a019786.

[95] Ding Z, Li M, Sun F, Xi P, Sun L, Zhang L, et al. Mitogen-activated protein kinases are associated with the regulation of physiological traits and virulence in Fusarium oxysporum f. sp. cubense. PLoS One. 2015;10(4):e0122634. doi:10.1371/journal.pone.0122634.

[96] Renshaw H, Vargas-Muñiz J, Juvvadi P, Richards A, Waitt G, Soderblom E, et al. The tail domain of the Aspergillus fumigatus class V myosin MyoE orchestrates septal localization and hyphal growth. J Cell Sci. 2018;131(3):jcs205955. doi:10.1242/jcs.205955.

[97] Schrettl M, Bignell E, Kragl C, Sabiha Y, Loss O, Eisendle M, et al. Distinct roles for intra- and extracellular siderophores during Aspergillus fumigatus infection. PLoS Pathog. 2007;3(9):1195–207. doi:10.1371/journal.ppat.0030128.

[98] White LO. Germination of Aspergillus fumigatus conidia in the lungs of normal and cortisone-treated mice. Sabouraudia,. 1977;Volume 15, Issue 1,:37–41. doi:https://doi.org/10.1080/00362177785190071.

[99] Sharif O, Bolshakov VN, Raines S, *et al* . Transcriptional profiling of the LPS induced NF-κB response in macrophages. BMC Immunol. 2007;8(1.). doi:doi.org/10.1186/1471-2172-8-1.

[100] Fritz K, Silvia M, Anne-Marie A, Gerlach JT, Jürgen B, Martina D. Cell Size of Alveolar Macrophages: An Interspecies Comparison. Environmental Health Perspectives. 1997;105(5):1261–1263. doi:10.2307/3433544.

[101] Trinci APJ. The hyphal growth unit of wild type and spreading colonial mutants of Neurospora crassa. Archiv Mikrobiol. 1973;91:127–136. doi:doi.org/10.1007/BF00424756.

[102] Goncalves SM, Lagrou K, Rodrigues CS, Campos CF, Bernal-Martinez L, Rodrigues F, et al. Evaluation of Bronchoalveolar Lavage Fluid Cytokines as Biomarkers for Invasive Pulmonary Aspergillosis in At-Risk Patients. Frontiers in Microbiology. 2017;8:2362. doi:10.3389/fmicb.2017.02362.

[103] Morgenstern DE, Gifford MAC, Li LL, Doerschuk CM, Dinauer MC. Absence of Respiratory Burst in X-linked Chronic Granulomatous Disease Mice Leads to Abnormalities in Both Host Defense and Inflammatory Response to Aspergillus fumigatus. Journal of Experimental Medicine. 1997;185(2):207–218. doi:10.1084/jem.185.2.207.

[104] Bonnett CR, Cornish EJ, Harmsen AG, Burritt JB. Early Neutrophil Recruitment and Aggregation in the Murine Lung Inhibit Germination of Aspergillus fumigatus Conidia. Infection and Immunity. 2006;74(12):6528–6539. doi:10.1128/IAI.00909-06.

[105] Dzhuraev G, Rodriguez-Castillo J, Ruiz-Camp J, Salwig I, Szibor M, Vadasz I, et al. Estimation of absolute number of alveolar epithelial type 2 cells in mouse lungs: a comparison between stereology and flow cytometry. Journal of Microscopy. 2019;275:36–50. doi:https://doi.org/10.1111/jmi.12800.

[106] Anh NH, Caroline NJ, Dimisko L, Hamza B, Martel J, Kojic N, et al. Measuring neutrophil speed and directionality during chemotaxis, directly from a droplet of whole blood. TECHNOLOGY. 2013;01(01):49–57. doi:doi.org/10.1142/S2339547813500040.

[107] Brandon M, Howard B, Lawrence C, Laubenbacher R. Iron acquisition and oxidative stress response in Aspergillus fumigatus. BMC systems biology. 2015;9(1):19.

[108] Irvin CG, Bates J. Measuring the lung function in the mouse: the challenge of size. Respiratory research. 2003;4(1). doi:10.1186/rr199.

[109] Knust J, Ochs M, Gundersen HJG, Nyengaard JR. Stereological Estimates of Alveolar Number and Size and Capillary Length and Surface Area in Mice Lungs. Anat Rec,. 2009;292:113–122. doi:10.1002/ar.20747.

[110] Mercer RR, Russell ML, Crapo JD. Alveolar septal structure in different species. Journal of Applied Physiology. 1994;7(3):1060–1066. doi:10.1152/jappl.1994.77.3.1060.

[111] Pollmächer J, Figge MT. Agent-based model of human alveoli predicts chemotactic signaling by epithelial cells during early Aspergillus fumigatus infection. PloS one. 2014;9(10):e111630.

[112] Schaffner A, Douglas H, Braude A. Selective protection against conidia by mononuclear and against mycelia by polymorphonuclear phagocytes in resistance to Aspergillus. Observations on these two lines of defense in vivo and in vitro with human and mouse phagocytes. J Clin Invest. 1982;69(3):617–631. doi:10.1172/jci110489.

[113] Ibrahim-Granet O, Philippe B, Boleti H, Boisvieux-Ulrich E, Grenet D, Stern M, et al. Phagocytosis and Intracellular Fate of ¡i¿Aspergillus fumigatus¡/i¿ Conidia in Alveolar Macrophages. Infection and Immunity. 2003;71(2):891–903. doi:10.1128/IAI.71.2.891-903.2003.

[114] Smedman C, Gårdlund B, Nihlmark K, Gille-Johnson P, Andersson J, Paulie S. ELISpot analysis of LPS-stimulated leukocytes: Human granulocytes selectively secrete IL-8, MIP-1β and TNF-α. Journal of Immunological Methods. 2009;346(1):1–8. doi:https://doi.org/10.1016/j.jim.2009.04.001.

[115] Meier A, Kirschning CJ, Nikolaus T, Wagner H, Heesemann J, Ebel F. Toll-like receptor (TLR) 2 and TLR4 are essential for Aspergillus-induced activation of murine macrophages. Cellular Microbiology. 2003;5(8):561–570. doi:https://doi.org/10.1046/j.1462-5822.2003.00301.x.

[116] Hentze M, Muckenthaler M, Andrews N. Balancing acts: molecular control of mammalian iron metabolism. Cell. 2004;117(3):285–297. doi:10.1016/s0092-8674(04)00343-5.

[117] Raychaudhuri B, Fisher CJ, Farver CF, Malur A, Drazba J, Kavuru MS, et al. INTERLEUKIN 10 (IL-10)-MEDIATED INHIBITION OF INFLAMMATORY CYTOKINE PRODUCTION BY HUMAN ALVEOLAR MACROPHAGES. Cytokine. 2000;12(9):1348–1355. doi:https://doi.org/10.1006/cyto.2000.0721.

[118] Soares M, Hamza I. Macrophages and Iron Metabolism. Immunity. 2016;44(3):1348–1355. doi:10.1016/j.immuni.2016.02.016.

[119] Dautry-Varsat A, Ciechanover A, Lodish HF. pH and the recycling of transferrin during receptor-mediated endocytosis. Proceedings of the National Academy of Sciences. 1983;80(8):2258–2262. doi:10.1073/pnas.80.8.2258.

[120] Fleming M, Andrews N. Mammalian iron transport: an unexpected link between metal homeostasis and host defense. J Lab Clin Med. 1998;132(6):464–8. doi:10.1016/s0022-2143(98)90123-8.

[121] Zu Y, Qi J, Gilchrist A, Fernandez G, Vazquez-Abad D, Kreutzer D, et al. p38 mitogen-activated protein kinase activation is required for human neutrophil function triggered by TNF-alpha or FMLP stimulation. J Immunol. 1998;160(4).

[122] Endo D, Saito T, Umeki Y, et al. Myeloperoxidase negatively regulates the expression of proinflammatory cytokines and chemokines by zymosan-induced mouse neutrophils. Inflamm Res. 2016;65:151–159. doi:https://doi.org/10.1007/s00011-015-0899-5.

[123] Li X, Cullere X, Nishi H, Saggu G, Durand E, Mansour MK, et al. PKC-d activation in neutrophils promotes fungal clearance. Journal of Leukocyte Biology. 2016;100(3):581–588. doi:https://doi.org/10.1189/jlb.4A0915-405R.

[124] Zarember ea K A. Human polymorphonuclear leukocytes inhibit Aspergillus fumigatus conidial growth by lactoferrin-mediated iron depletion. J Immunol. 2007;178:6367–73.

[125] Gazendam R, van Hamme J, Tool A, Hoogenboezem M, van den Berg J, Prins J, et al. Human Neutrophils Use Different Mechanisms To Kill Aspergillus fumigatus Conidia and Hyphae: Evidence from Phagocyte Defects. J Immunol. 2016;196(3):1272–1283. doi:10.4049/jimmunol.1501811.

[126] Chen F, Zhang C, Jia X, Wang S, Wang J, Chen Y, et al. Transcriptome Profiles of Human Lung Epithelial Cells A549 Interacting with Aspergillus fumigatus by RNA-Seq. PLoS ONE. 2015;10(8):e0135720. doi:https://doi.org/10.1371/journal.pone.0135720.

[127] Bellanger AP, Millon L, Khoufache K, Rivollet D, Bièche I, Laurendeau I, et al. Aspergillus fumigatus germ tube growth and not conidia ingestion induces expression of inflammatory mediator genes in the human lung epithelial cell line A549. Journal of Medical Microbiology. 2009;58(2):174–179. doi:https://doi.org/10.1099/jmm.0.005488-0.

[128] Zhang Z, Liu R, Noordhoek J, Kauffman H. Interaction of airway epithelial cells (A549) with spores and mycelium of Aspergillus fumigatus. The Journal of infection. 2006;51:375–82. doi:10.1016/j.jinf.2004.12.012.

[129] Sharma AK, Fernandez LG, Awad AS, Kron IL, Laubach VE. Proinflammatory response of alveolar epithelial cells is enhanced by alveolar macrophage-produced TNF-α during pulmonary ischemia-reperfusion injury. American Journal of Physiology-Lung Cellular and Molecular Physiology. 2007;293(1):L105–L113. doi:10.1152/ajplung.00470.2006.

[130] Schrettl M, Bignell E, Kragl C, Joechl C, Rogers T, Arst J Herbert N, et al. Siderophore Biosynthesis But Not Reductive Iron Assimilation Is Essential for Aspergillus fumigatus Virulence. J Exp Med. 2004;200(9):1213–1219. doi:10.1084/jem.20041242.

[131] Mazurier J, Spik G. Comparative study of the iron-binding properties of human transferrins: I. Complete and sequential iron saturation and desaturation of the lactotransferrin. Biochimica et Biophysica Acta (BBA) - General Subjects. 1980;629(2):399–408. doi:https://doi.org/10.1016/0304-4165(80)90112-9.

[132] Gordon S. Alternative activation of macrophages. Nat Rev Immunol. 2003;3:23–35. doi:https://doi.org/10.1038/nri978.

[133] Arango Duque G, Descoteaux A. Macrophage Cytokines: Involvement in Immunity and Infectious Diseases. Frontiers in Immunology. 2014;5:491. doi:10.3389/fimmu.2014.00491.